AD_____

Award Number: W81XWH-08-1-0537

TITLE: FoxP3 as a missing link between inflammation and breast cancer

PRINCIPAL INVESTIGATOR: Yang Liu, Ph.D.

CONTRACTING ORGANIZATION: The University of Michigan
Ann Arbor, MI 48109

REPORT DATE: September 2011

TYPE OF REPORT: Revised Annual

PREPARED FOR: U.S. Army Medical Research and Materiel Command
Fort Detrick, Maryland 21702-5012

REPORT DOCUMENTATION PAGE

Form Approved
OMB No. 0704-0188

1. REPORT DATE *(DD-MM-YYYY)*	2. REPORT TYPE	3. DATES COVERED *(From - To)*
September 2011	Revised Annual	1 September 2010 - 31 August 2011

4. TITLE AND SUBTITLE
FoxP3 as a missing link between inflammation and breast cancer

5a. CONTRACT NUMBER

5b. GRANT NUMBER
W81XWH-08-1-0537

5c. PROGRAM ELEMENT NUMBER

6. AUTHOR(S)
Yang Liu, Ph.D.

E-Mail: yangl@umich.edu

5d. PROJECT NUMBER

5e. TASK NUMBER

5f. WORK UNIT NUMBER

7. PERFORMING ORGANIZATION NAME(S) AND ADDRESS(ES)
The University of Michigan
Ann Arbor, MI 48109

8. PERFORMING ORGANIZATION REPORT NUMBER

9. SPONSORING / MONITORING AGENCY NAME(S) AND ADDRESS(ES)
U.S. Army Medical Research and Materiel Command
Fort Detrick, Maryland 21702-5012

10. SPONSOR/MONITOR'S ACRONYM(S)

11. SPONSOR/MONITOR'S REPORT NUMBER(S)

12. DISTRIBUTION / AVAILABILITY STATEMENT
Approved for Public Release; Distribution Unlimited

13. SUPPLEMENTARY NOTES

14. ABSTRACT

This is the third annual report. The major achievement is establishment of a new mechanism by which Foxp3 activates gene expression. Both H4K16 acetylation and H3K4 tri-methylation are required for gene activation. However, it is still largely unclear how these modifications are orchestrated by transcriptional factors. Here we analyzed the mechanism of the transcriptional activation by FOXP3, an X-linked suppressor of autoimmune diseases and cancers. FOXP3 binds near transcriptional start sites of its target genes. By recruiting MOF and displacing histone H3K4 demethylase PLU-1, FOXP3 increases both H4K16 acetylation and H3K4 tri-methylation at the FOXP3-associated chromatins of multiple FOXP3-activated genes. RNAi-mediated silencing of MOF reduced both gene activation and tumor suppression by FOXP3, while both somatic mutations in clinical cancer samples and targeted mutation of FOXP3 in mouse prostate epithelial disrupted nuclear localization of MOF. Our data demonstrate a pull-push model in which a single transcription factor orchestrates two epigenetic alterations necessary for gene activation and provide a mechanism for somatic inactivation of the FOXP3 protein function in cancer cells.

15. SUBJECT TERMS
Inflammation, FoxP3, breast cancer risk

16. SECURITY CLASSIFICATION OF:			17. LIMITATION OF ABSTRACT	18. NUMBER OF PAGES	19a. NAME OF RESPONSIBLE PERSON
a. REPORT	b. ABSTRACT	c. THIS PAGE			USAMRMC
U	U	U	UU	36	19b. TELEPHONE NUMBER *(include area code)*

Table of Contents

(4) Introduction

We have received approval to revise the Tasks (SOW) of the award. The new tasks as approved are as follows.

In **task 1**, *we will use systemic approach to define the cytokines genes regulated by Foxp3 expression in normal and malignant breast epithelial cells*.

*In **task.2**, we propose to study the significance of FOXP3-induced cytokines in innate and adaptive immunity to breast cancer.*

*In **task 3,** we will determine Foxp3-repressed cytokines.*

In the last report, we have reported progress on part of task 1. In the last funding period, we have completed task 1, and produced a manuscript that is published in Molecular Cell. Another related manuscript has been published in Cancer Research. We have also initiated studies in tasks 2 and 3. However, due to slow approval of animal studies, we were not able to carry out in vivo studies. Therefore, we have decided to request a no cost extension for one more year.

(5) Body of Annual Report

Statement of work

In **task 1**, *we will use systemic approach to define the cytokines genes regulated by Foxp3 expression in normal and malignant breast epithelial cells*.
In the previous funding period, we have reported our effort in global analysis of Foxp3-mediated expression of cytokines. Therefore, we devoted a major effort to understand at the global level how FOXP3 regulates its target genes.

Acetyl-H4 is an important histone mark for gene activation, and a previous study reported that FOXP3 directly or indirectly mediates acetylation of pan-histone H4 in T cells (1). Histone H4 has various lysine residues which can be substrates for acetylation and, among them, H4K16ac is a founder event of the H4 acetylation (2). In order to investigate whether or not the H4K16ac is correlated with FOXP3-mediated gene activation in MCF7 cells, we compared H4K16ac levels at FOXP3 binding sites before and after FOXP3 induction. Surprisingly, ChIP-qPCR at FOXP3 binding sites of randomly chosen 4 activated (including the previously reported *p21* gene) and 3 repressed promoters demonstrated broad inductions of H4K16ac by FOXP3 regardless of whether the genes were activated or repressed (Fig. 1A). To substantiate the broad correlation between FOXP3 binding and H4K16ac, we performed a confocal imaging analysis. As shown in Fig. 1B and 1C, FOXP3 and H4K16ac exhibited an almost complete overlap throughout the nuclei of the MCF7 cells.

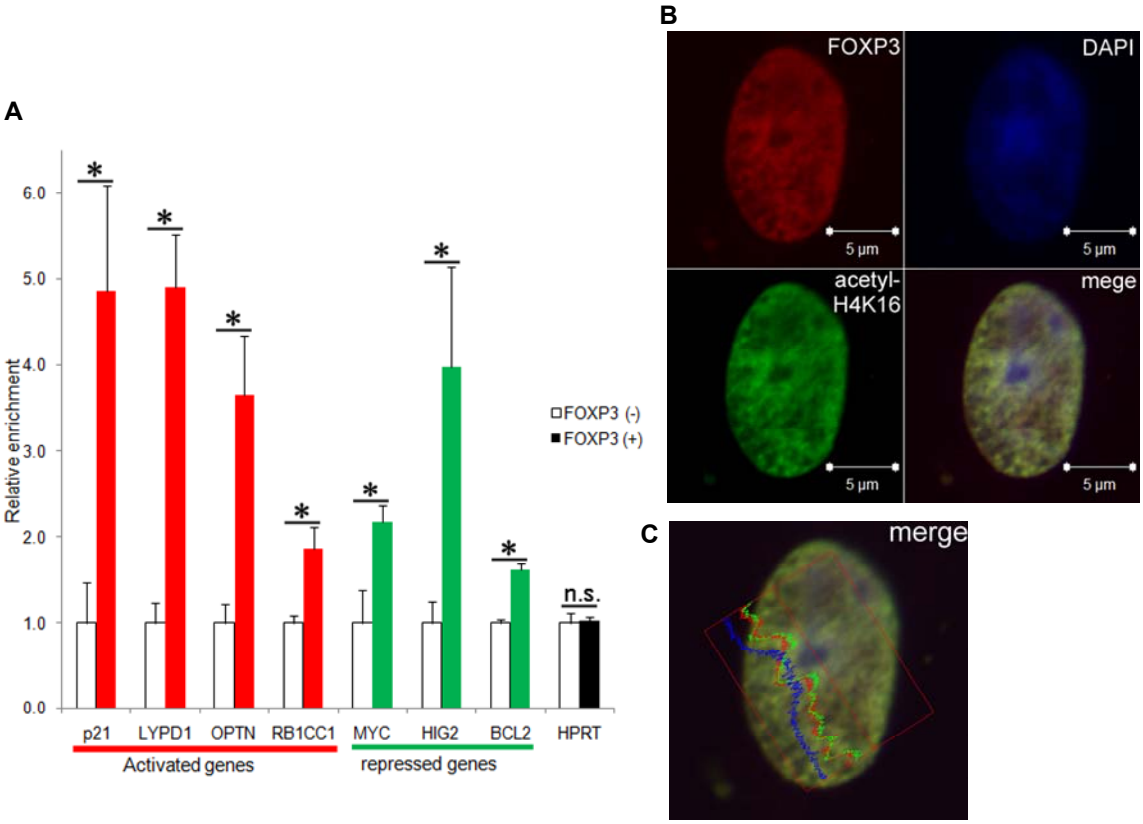

Figure 1. H4K16ac is induced by FOXP3-binding. (A) H4K16ac levels at FOXP3 binding sites were examined by ChIP-qPCR before and after FOXP3 induction in the FOXP3-tet-off MCF7 cell. Y-axis represents enrichments of the H4K16ac (% of input DNA). Error bars represent +1SD of triplicate qPCR. *: $p<0.05$ (t-test). n.s.: not significant. (B) A representative confocal image of FOXP3 (red) and H4K16ac (green) in the MCF7 cell transfected with FOXP3. White bars represent 5μm. Similar pattern was observed in 10/10 cells analyzed. (C) A representative signal intensity profile in the confocal image (Fig. 2B) is shown. Red, green and blue graphs indicate signal intensities of FOXP3, H4K16ac and DAPI, respectively.

In order to investigate whether MOF is required for FOXP3-dependent gene activation, we treated FOXP3-tet-off MCF7 cells with RNAi duplexes targeting endogenous MOF or control RNAi duplex (Fig. 4A). In this model, induced FOXP3 expression was identical between control RNAi and MOF-RNAi treated cells both in protein and mRNA levels. Global mRNA expression analysis revealed that endogenous MOF knockdown impaired FOXP3-dependent gene activation in most, if not all, of the direct target genes (Fig. 2A). Approximately 41.0% of target genes showed more than 30% impairment of FOXP3-mediated gene activation by MOF-RNAi as compared to control-RNAi. In contrast, in FOXP3-mediated gene repression, the affected gene numbers and magnitudes of impairments by the MOF knockdown seemed to be considerably smaller (Fig. 2B). Thus, at global level, MOF plays a more important role in FOXP3-mediated gene activation than in gene repression.

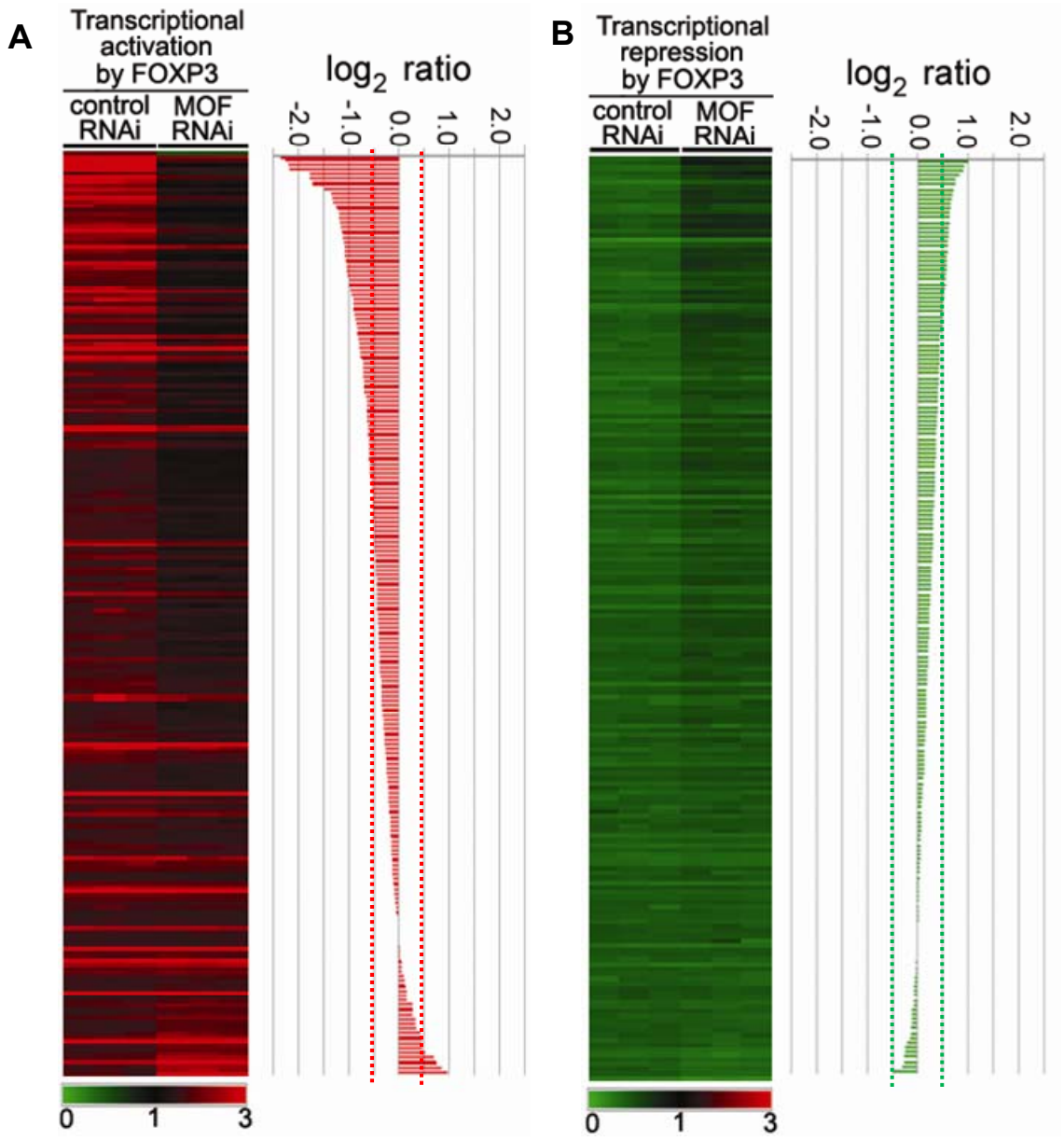

Fig. 2. Global mRNA expression analysis of direct target genes of FOXP3 with and without MOF knockdown. RNAi #2 was used in this analysis as the knockdown is more efficient. A. The heat map represents ratios of mRNA expressions before and after FOXP3 induction in control-RNAi and MOF-RNAi treated MCF7 cells (expression values in cells without FOXP3 induction were normalized to 1.0). Color scale of the heat map is indicated at the bottom of the figure. B**.** Bar graph represents log-scaled ratio of the relative mRNA expression between control-RNAi and MOF-RNAi groups. Dashed lines (red and green) represent log (ratio) = +0.5 (ratio=1.41) and = -0.5 (ratio=0.71). The "direct target genes" were defined as (1) direct binding of FOXP3 between -2 kbp and +2 kbp from TSS of genes revealed by ChIP-seq, and (2) mRNA expression values were increased to more than 1.5 times or decreased to less than 2/3 after FOXP3 induction in the control-RNAi treated MCF7 cells. Ctrl: control.

In order to explain how FOXP3 induces H3K4me3 at its activating binding sites, we carried out a motif scanning of the FOXP3-bound regions and searched for any enriched DNA motifs among activating and repressing binding sites. Apart from the FOXP3-binding motif (forkhead motif), the most enriched motif in the activated binding sites was a PLU-1-binding motif (Fig. 3A). Interestingly, PLU-1 is a H3K4me3 demethylase and a putative oncogene for breast cancer (3). Importantly, the enrichment of the PLU-1 motif was specific in FOXP3's activating binding sites (Fig. 3A). PLU-1 has a known DNA-binding motif (Fig. 3B) (4). Strikingly, DNA binding motifs of FOXP3 and PLU-1 were enriched at essentially overlapping regions (Fig. 3C). This close proximity suggested a model in which FOXP3 binding would competitively displace PLU-1 from FOXP3-associated chromatin.

A

Enriched Transcription Factor Binding Motif among activated gene promoters.

TF Matrices	Transcription factor	Over representation	*Z*-Score
V$HNF3.01	FOXP3 (Fork Head motif)	2.51	6.05
V$PLU1_JARID1B.01	PLU-1	2.28	4.5
V$NUDR.01	NUDR	1.95	4.3
V$USF.01	USF	1.9	3.57
V$ZBRK1.01	ZBRK	1.89	2.68
V$HIVEP1.01	HIVEP1	1.88	4.02
V$SZF1.01	SZF1	1.84	2.54
V$NFKAPPAB.02	NFκB	1.82	3.75
V$E2F1_DP1.01	E2F	1.81	3.17
V$USF.02	USF	1.81	3.16

Enriched Transcription Factor Binding Motif among repressed gene promoters.

TF Matrices	Transcription factor	Over representation	*Z*-Score
V$HFH3.01	FOXP3 (Fork Head motif)	3.42	3.37
V$PAX4_PD.01	PAX4	3.19	2.64
V$VMAF.01	MAF	3.02	3.41
V$GRHL1.01	Grainyhead-like 1	3	5.1
V$AP1.03	AP1	2.7	3.35
V$AHRARNT.01	Aryl hydrocarbon receptor	2.68	3.15
V$TEF1.01	TEF-1	2.6	4.49
V$AHRARNT.03	Aryl hydrocarbon receptor	2.53	3.65
V$RB_E2F1_DP1.01	E2F	2.5	3.34
V$AP1.01	AP1	2.49	3.46

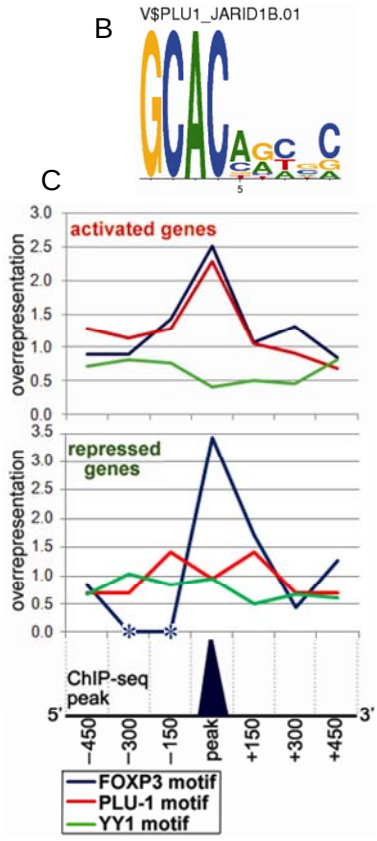

Figure 3. Bioinformatic analysis suggest that FOXP3 facilitates H3K4me3 presumably by replacing histone demethylase(s) from its binding sites: a hypothetical model. **(A)** Transcription factor binding motifs which were significantly enriched among FOXP3-binding sites at either activated or repressed gene promoters are listed. TOP-10 ranked motifs as sorted by overrepresentation scores were included. Statistical significances were evaluated by Z-score according to the database www.genomatix.de. **(B)** A known DNA binding motif of PLU-1. **(C)** Genomic regions around the FOXP3-ChIP-seq peaks were partitioned into 150 bp windows, and enrichments of the Fork Head (FOXP3) and PLU-1 motifs among each of these 150 bp partitions are evaluated by the

overrepresentation scores as in Fig. 3A. The YY1 motif was used as an unrelated negative control. *: Fork Head motifs were not identified in these regions.

To test this model, we evaluated whether FOXP3 binding reduced enrichments of PLU-1 at FOXP3 binding sites. Fifteen activated and 11 repressed genes were chosen according to the following criteria: (1) genes whose expression were strongly affected by FOXP3 (more than twice or less than half compared to FOXP3(-) cells) and (2) both of the FOXP3 and PLU-1 motifs were identified around ChIP-seq peaks (within 500 bp of the ChIP-seq peaks). As shown in Figure 7D, induction of FOXP3 significantly reduced the binding of PLU-1 at 9 out of 15 activated promoters. FOXP3 and PLU-1 motifs were essentially overlapped at *p21*, *YPEL2* and *ITGB8* promoters and located closely at other promoters. Interestingly, the distance between FOXP3 and PLU-1 motifs is likely a major contributor for the competitive displacements of PLU-1 by FOXP3, as all 9 genes that showed significant displacements of PLU-1 had FOXP3 motifs within 100 bp from the PLU-1 motif. However, proximity of the binding sites is not sufficient since displacements were not observed in 2 genes with the distance less than 100 bp. Importantly, no displacements of PLU-1 were observed among repressed genes (Fig. 4). Since JARID1 family members may not always bind to chromatin in a DNA sequence-specific fashion, it is possible that, at the repressed promoters, PLU-1 binds to other chromatin-associated proteins and is not competitively displaced by FOXP3.

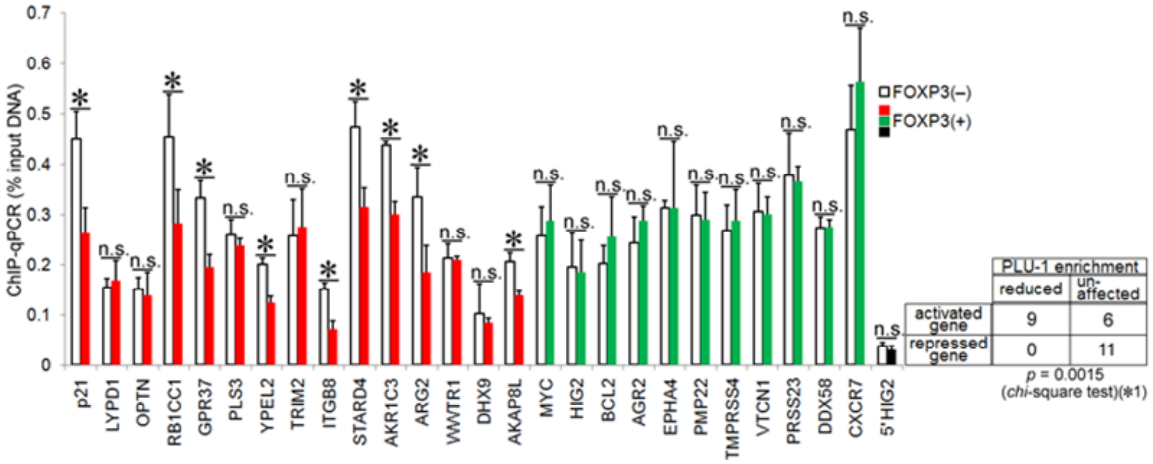

Taken together, based on ChIP seq data and analysis of epigenetic alterations of FOXP3 targets, we established a novel mechanism on how FOXP3 regulate gene expression. We showed that, By recruiting MOF and displacing histone H3K4 demethylase PLU-1, FOXP3 increases both H4K16 acetylation and H3K4 tri-methylation at the FOXP3-associated chromatins of multiple FOXP3-activated genes. RNAi-mediated silencing of *MOF* reduced both gene activation and tumor suppression by FOXP3, while both somatic mutations in clinical cancer samples and targeted mutation of FOXP3 in mouse prostate epithelial disrupted nuclear localization of MOF. Our data demonstrate a pull-push model in which a single transcription factor orchestrates two epigenetic alterations necessary for gene activation and provide a mechanism for somatic inactivation of the FOXP3 protein function in cancer cells, as shown in Fig. 5.

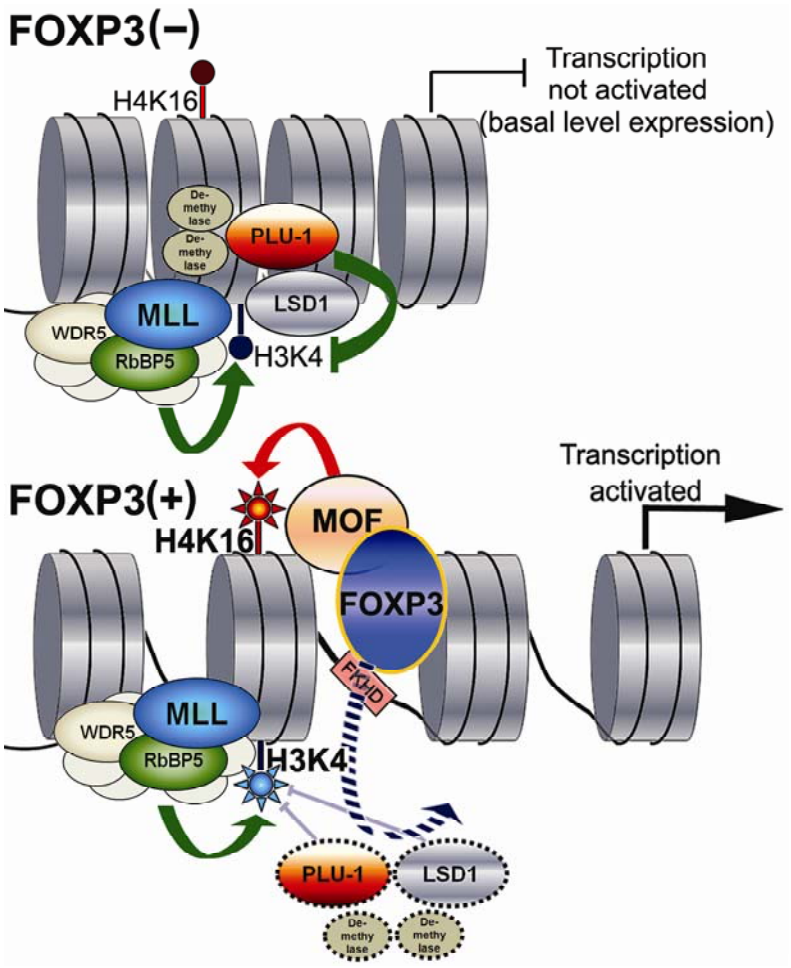

Fig. 5. A proposed model by which FOXP3 activates multiple gene expression by pulling MOF and causing displacement of H3K4me demethylase(s). The data supporting the model has been accepted for publication in Molecular Cell.

(6) Key Research Accomplishments

We have completed a major analysis on global mechanism of FOXP3-mediated gene regulation. The data may provide a new paradigm on how a transcription factor controls local histone modifications and thus recruiting chromatin-remodeling complexes. This mechanism will be applied to our analysis on how foxp3 regulates inflammation as many of the Foxp3 targets are inflammatory cytokines.

(7) Reportable Outcomes:

Manuscripts:

1. Weiquan Li, Lizhong Wang, Hiroto Katoh, Runhua Liu, Pan Zheng, and **Yang Liu** Identification of a Tumor Suppressor Relay between the FOXP3 and the Hippo Pathways in Breast and Prostate Cancers. Cancer Research 71:2162-2171 (2011).
2. . Hiroto Katoh, Zhaohui S. Qin, Runhua Liu, Lizhong Wang, Weiquan Li, Xiangzhi Li, Lipeng Wu, Robert Lyons, Chang-Gong Liu, Xiuping Liu, Yali Dou, Pan Zheng, **Yang Liu** FOXP3 Orchestrates H4K16 Acetylation and H3K4 Tri-Methylation for

Gene Activation through Recruiting MOF and Causing Displacement of PLU-1. Molecular Cell (In Press).

(8) Conclusions and future plan:

Our global analysis of FOXP3 targets not only reveal their identity but also raised fundamental questions on how FOXP3 can regulate a large array of targets directly. The mechanism identified will have direct relevance on how FOXP3 in cancer cell regulate inflammation. We plan to complete the new tasks 2 and 3 in the coming year.

(9) References:

1. **Pan F, *et al.* (2009) Eos mediates Foxp3-dependent gene silencing in CD4+ regulatory T cells. *Science* 325(5944):1142-1146**
2. **Dion MF, Altschuler SJ, Wu LF, & Rando OJ (2005) Genomic characterization reveals a simple histone H4 acetylation code. *Proc. Natl. Acad. Sci. U. S. A.* 102(15):5501-5506**
3. **Yamane K, *et al.* (2007) PLU-1 is an H3K4 demethylase involved in transcriptional repression and breast cancer cell proliferation. *Mol. Cell* 25(6):801-812**
4. **Scibetta AG, *et al.* (2007) Functional analysis of the transcription repressor PLU-1/JARID1B. *Mol. Cell. Biol.* 27(20):7220-7235**

Published OnlineFirst January 28, 2011; DOI:10.1158/0008-5472.CAN-10-3268

Molecular and Cellular Pathobiology

Cancer Research

Identification of a Tumor Suppressor Relay between the FOXP3 and the Hippo Pathways in Breast and Prostate Cancers

Weiquan Li[1], Lizhong Wang[1], Hiroto Katoh[1], Runhua Liu[1], Pan Zheng[1,2], and Yang Liu[1,3]

Abstract

Defective expression of *LATS2*, a negative regulator of YAP oncoprotein, has been reported in cancer of prostate, breast, liver, brain, and blood origins. However, no transcriptional regulators for the *LATS2* gene have been identified. Here we report that spontaneous mutation of the transcription factor *FOXP3* reduces expression of the *LATS2* gene in mammary epithelial cells. shRNA-mediated silencing of *FOXP3* in normal or malignant mammary epithelial cells of mouse and human origin repressed *LATS2* expression and increased YAP protein levels. *LATS2* induction required binding of FOXP3 to a specific sequence in the *LATS2* promoter, and this interaction contributed to FOXP3-mediated growth inhibition of tumor cells. In support of these results, reduced expression and somatic mutations of *FOXP3* correlated strongly with defective *LATS2* expression in microdissected prostate cancer tissues. Thus, defective expression of *LATS2* is attributable to FOXP3 defects and may be a major independent determinant of YAP protein elevation in cancer. Our findings identify a novel mechanism of LATS2 downregulation in cancer and reveal an important tumor suppressor relay between the FOXP3 and HIPPO pathways which are widely implicated in human cancer. *Cancer Res; 71(6); 2162–71.* ©*2011 AACR.*

Introduction

Genetic studies in *Drosophila* have established an important role for the *Hippo* pathway in regulation of cell proliferation and apoptosis (1–3). Components of the Hippo pathway, including Yap, Lats1/2, and Mst1/2 (*Drosophila Yki*, *Hpo*, and *Wts* homologs, respectively) are highly conserved between Drosophila and human, as the human *YAP*, *LATS2*, and *MST2* are capable of rescuing the corresponding *Drosophila* mutants (1, 3). The functional conservation raised the possibility that the *Lats1* and *Lats2*, the mammalian *Wts* homologs may function as tumor suppressors. In support of this notion, targeted mutation of *Lats1* caused soft-tissue tumor in the mice (4). Although *Lats2* deletion is embryonic lethal, analysis of the *Lats2*$^{-/-}$ murine embryonic fibroblast suggests a critical role of Lats2 in genome stability and growth inhibition (5). Recent studies have revealed that *LATS2* regulates cellular localization (6, 7) and degradation (8) of YAP protein. Transgenic expression of an active Yap mutant lacking a Lats2 phosphorylate site caused liver cancer (6). The significance of *LATS2* in human cancer is supported by widespread downregulation of *LATS2* in cancers in breast (9), prostate (10), brain (11), and blood (12). However, genetic lesions that disrupt the LATS2 expression have not yet been identified.

FOXP3 is a newly identified X-linked tumor suppressor gene for both prostate and breast cancers (13, 14). Our recent studies have shown that, as a transcriptional factor, Foxp3 inhibits tumor cell growth by both repressing oncogenes, *Erbb2* (14), *cMyc* (13), and *Skp2* (15) and inducing tumor suppressor *p21* (16). Here we report that Foxp3 is a direct transcriptional activator for *Lats2* in both normal and malignant breast and prostate cells from mouse and human. Mutation or downregulation of Foxp3 decreased Lats2 expression. These data show a functional relay between 2 newly identified tumor suppressor genes.

Materials and Methods

Mice

Rag2$^{-/-}$*Foxp3*$^{+/+}$ and *Rag2*$^{-/-}$*Foxp3*$^{sf/sf}$ female and male *Rag2*$^{-/-}$*Foxp3*$^{+/y}$ and *Rag2*$^{-/-}$*Foxp3*$^{sf/y}$ male BALB/c mice have been described previously (17). Four-month-old virgin mice were used to analyze the effect of *Foxp3* mutation on *Lats2* expression and hyperplasia of mammary epithelia. All animal experiments were conducted in accordance with accepted standards of animal care and approved by the Institutional Animal Care and Use Committee of University of Michigan.

Authors' Affiliations: Departments of [1]Surgery, [2]Pathology, and [3]Internal Medicine, Division of Immunotherapy, University of Michigan School of Medicine and Cancer Center, Ann Arbor, Michigan

Note: Supplementary data for this article are available at Cancer Research Online (http://cancerres.aacrjournals.org/).

Corresponding Author: Yang Liu, University of Michigan, BSRB 2059, 109 Zina Pitcher Place, Ann Arbor, MI 48109. Phone: 734-615-3158; Fax: 734-763-2162; E-mail: yangl@umich.edu

doi: 10.1158/0008-5472.CAN-10-3268

Published OnlineFirst January 28, 2011; DOI:10.1158/0008-5472.CAN-10-3268

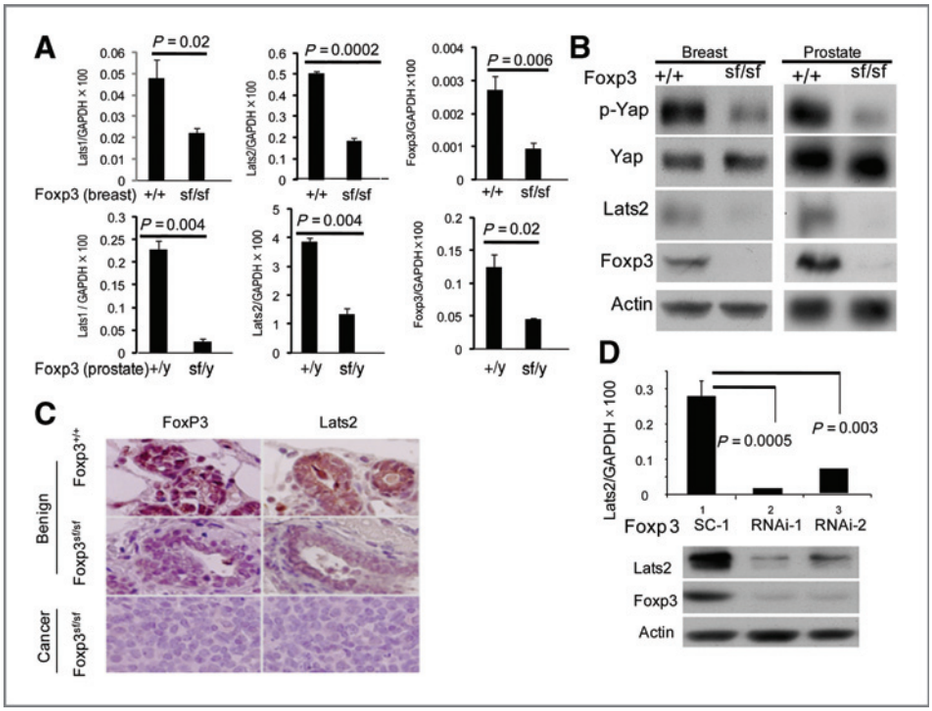

Figure 1. Foxp3 induced Lats2 expression in normal and malignant mammary epithelial cells in the mice. A, mouse mammary (top) and prostate (bottom) epithelial cells were isolated from *Rag2*$^{-/-}$*Foxp3*$^{+/+}$ and *Rag2*$^{-/-}$*Foxp3*$^{sf/sf}$ mammary glands or *Rag2*$^{-/-}$*Foxp3*$^{+/y}$ and *Rag2*$^{-/-}$*Foxp3*$^{sf/y}$ prostate. *Lats1*, *Lats2*, and *Foxp3* mRNA levels were determined by real-time RT-PCR. Data shown were mean ± SD of mRNA levels presented as %GAPDH and have been repeated 3 times. B, Foxp3 regulates Lats2, Yap protein levels, and Yap phosphorylation (Yap-pS127), as shown by Western blot. The results have been repeated 3 times. C, immunohistochemical analysis for Lats2 protein expression in benign mammary tissue from WT and Foxp3 mutant mice, as well as a mammary tumor of *Rag2*$^{-/-}$*Foxp3*$^{sf/sf}$ origin. D, Foxp3 regulates expression of the *Lats2* gene in mouse mammary tumor cell line. *Lats2* mRNA in murine mammary tumor cell line TSA transfected with either scrambled or *Foxp3* siRNA. Transfected cells were selected by puromycin for 2 weeks after transfection. The results have been repeated 3 times.

Cell culture

Breast cancer cell line MCF-7 was purchased from the American Type Culture Collection and immortalized mammary epithelial cell line MCF-10A was obtained from Dr. Ben Margolis (University of Michigan). A Tet-off *FOXP3* expression system in the MCF-7 cells has been established previously (14). Cell banks were created after cells were received. Early passages of cells were used for the study. No reauthentification of cells has been done since receipt.

FOXP3 silencing

The human *FOXP3* silencing vectors were described previously (16). The mouse *Foxp3* shRNA and control lentiviral vectors pLKO.1 were purchased from Open Biosystems.

Western blot

The anti-FOXP3 (hFOXY; eBioscience; 1:100), anti-Lats2 (Cell Signaling; 1:1,000), anti-Yap, anti–p-Yap(Cell Signaling) and anti–β-actin (Sigma, 1:3,000) were used as primary antibodies. Anti-rabbit or mouse immunoglobulin G (IgG) horseradish peroxidase–linked secondary antibody at 1:3,000 to 1:5,000 dilutions (Cell Signaling) was used.

Chromatin immunoprecipitation

Chromatin immunoprecipitation (ChIP) was carried out according to the published procedure (16). Briefly, the FOXP3-transfected Tet-off cells were sonicated and fixed with 1% paraformaldehyde. The anti-FOXP3, and anti-IgG (Santa Cruz Biotechnology) antibodies were used to pull down chromatin associated with FOXP3. The amounts of the specific DNA fragment were quantitated by real-time PCR and normalized against the genomic DNA preparation from the same cells. The ChIP real-time PCR primers are listed in Supplementary Table S1.

Quantitative real-time PCR

Relative quantities of mRNA expression were analyzed by real-time PCR (ABI Prism 7500 Sequence Detection System; Applied Biosystems). The SYBR (Applied Biosystems) green fluorescence dye was used in this study. The primer sequences are listed in the Supplementary Table S1.

Tumorigenicity assay

TSA cells (10^6 per inoculation) were injected into mammary fat pads of syngeneic BALb/c mice. The tumor volumes are defined as $0.75\pi r^3$, where r is radius. The tumor diameters

Published OnlineFirst January 28, 2011; DOI:10.1158/0008-5472.CAN-10-3268

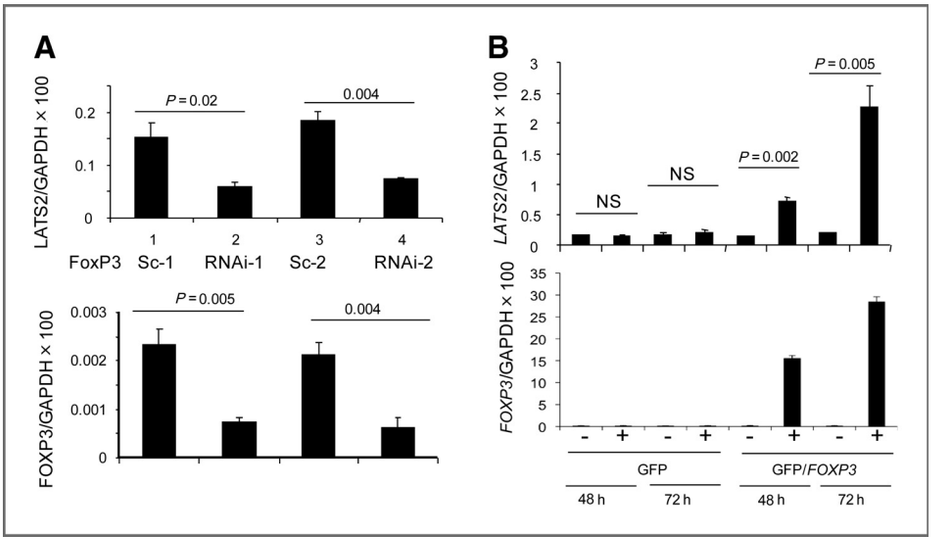

Figure 2. *FOXP3* is necessary and sufficient for expression of *LATS2* gene in normal and malignant human mammary epithelial cells. A, silencing *FOXP3* in MCF10A cells reduces *LATS2* expression. The levels of *FOXP3* (top) and *LATS2* (bottom) in 2 scrambled or 2 *FOXP3* siRNA-transfected cells as determined by real-time RT-PCR. Data shown are mean ± SD of 3 independent experiments. B, induction of *LATS2* mRNA by *FOXP3* in MCF7 Tet-off system. MCF7 cells with Tet-off expression of either GFP control or GFP in conjunction with FOXP3 were cultured for 48 or 72 hours in the absence of doxycyclin. The *LATS2* mRNA was quantified by real-time PCR. The induction of *FOXP3* mRNA is shown at the bottom. Data shown are mean ± SD of 3 independent experiments.

were derived from the average of largest diameters in two dimensions.

Site-directed mutagenesis

All mutants were generated by using mutgenesis kit from Stratagene (catalog no. 210518). The deleted sequence *LATS2* promoter mutants were ATAACAT for B6M, CAGTTGT for B7M, and TGTTTAT for B8M.

Immunohistochemistry

Immunohistochemistry was done by the avidin–biotin complex method. Expression of FOXP3 in human breast cancer or normal tissue samples was determined by immunohistochemistry, as described (13). The rabbit anti-Lats2 monoclonal antibody (Cell Signaling; 1:200), and biotinylated goat anti-mouse IgG were obtained from Santa Cruz and used at 1:200. FOXP3 and Lats2 staining of tissue microarray (TMA) samples (US Biomax, Inc.) were scored double blind.

DNA sequencing for human *YAP* gene in prostate cancer samples

To test whether human *YAP* is somatically mutated in primary prostate cancer samples to gain resistance to regulation by LATS, we sequenced exons 2 and 6 of human *YAP*, which encodes amino acid sequence encompassing S127 and S347 (S381) sites, respectively. DNA were prepared from microdissected normal and cancerous prostate tissues from the same patients. The genomic DNA were amplified by PCR by using a forward primer (AACCTGTGTTCTCCAGTGTCG) and a reverse primer (ATGTCTTTGCCATCTCCCAA) for exon 2; and a forward primer (AGAGCTGCCAGCTTCAATTA) and a reverse primer (ACCCGGCCAATCCATGATAT) for exon 6. The PCR products were sequenced. When ambiguous results were obtained, the DNA will be cloned and sequenced. At least 5 clones were analyzed per sample.

Statistical analysis

Data are shown as mean ± SD. Statistical analysis was performed with Student's *t* test. ANOVA tests were used to analyze data with more than 2 groups. Chi-square test was used to determine statistical significance of relationship between the expression of *FOXP3* and *LATS2*.

Results

Requirement for *Foxp3* in the expression of *Lats2* in both normal and malignant breast epithelia

Our gene array analysis showed that induction of *FOXP3* in breast cancer cell line MCF7 leads to increased *LATS2* expression (16). To determine whether endogenous *Foxp3* regulates *Lats2* in murine mammary epithelial cells, we used the Scurfy (sf) mice with a spontaneous mutation of the X-linked *Foxp3* gene (a dinucleotide insertion, $Foxp3^{sf}$) to determine the impact of *Foxp3* inactivation on the expression of *Lats2*. Because the homozygous mutation caused lethal autoimmune diseases in the immune competent mice, we crossed the mutation into $Rag^{-/-}$ mice that lack T and B cells. We isolated mammary epithelial cells from $Rag2^{-/-}Foxp3^{+/+}$ and $Rag2^{-/-}Foxp3^{sf/sf}$ mice and prostate epithelial cells from $Rag2^{-/-}Foxp3^{+/y}$ and $Rag2^{-/-}Foxp3^{sf/y}$ mice and compared the level of *Lats1* and *Lats2* transcripts by real-time PCR. As shown in Figure 1A (top), epithelial preparation from the $Foxp3^{sf/sf}$ mice showed a

Published OnlineFirst January 28, 2011; DOI:10.1158/0008-5472.CAN-10-3268

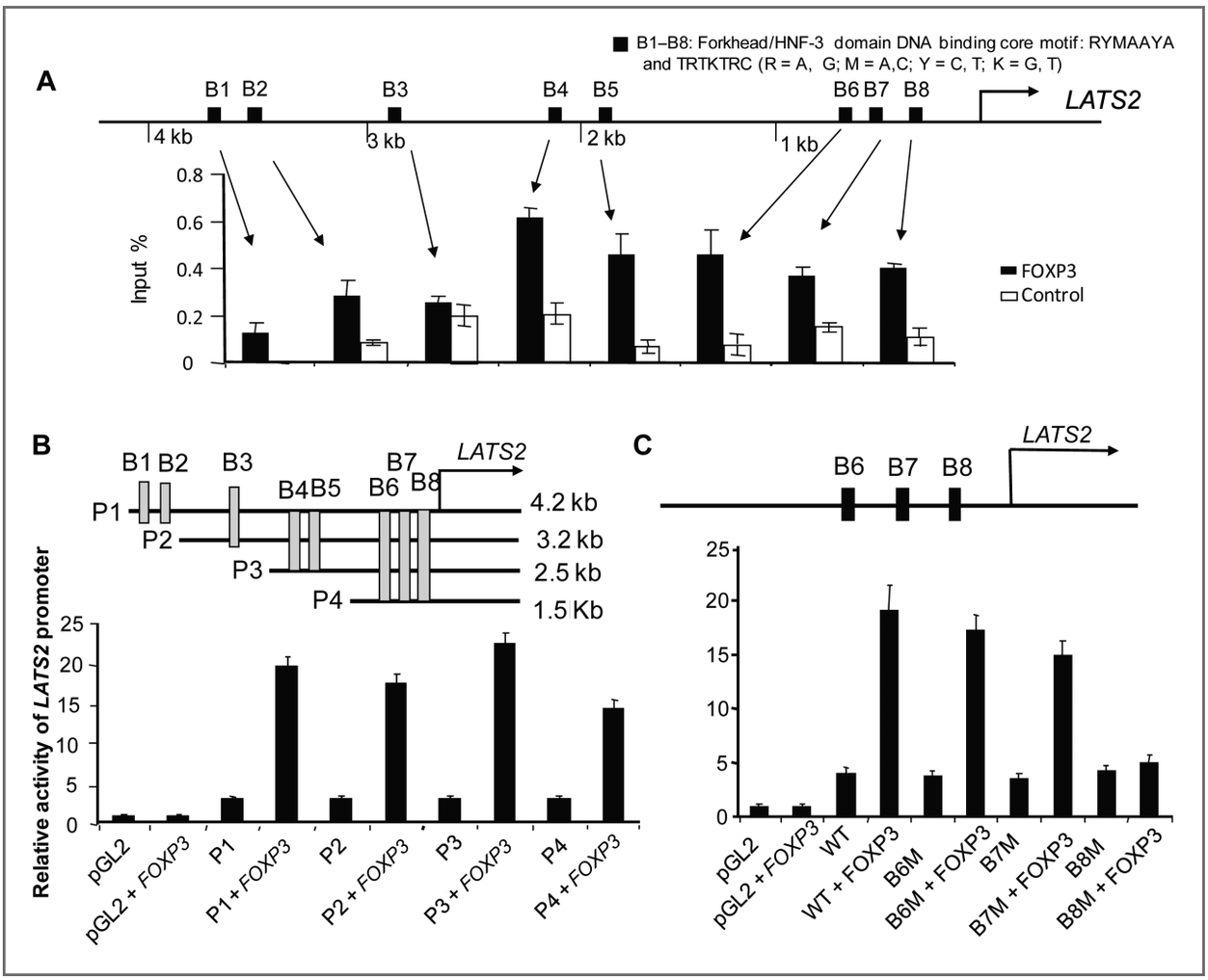

Figure 3. Identification of an essential *cis* element in *LATS2* gene responsible for FOXP3-mediated transcriptional activation. A, identification of FOXP3 binding sites by ChIP analysis. FOXP3 was induced in MCF7 Tet-off system by removing doxycycline for 2 days. The induced MCF7 cells were lysed in ChIP buffer to prepare chromatin for immunoprecipitation by anti-FOXP3 antibody. Top, the Forkhead binding motif, as marked by B1 to B8; bottom, the percent of input DNA precipitated by anti-FOXP3 or control IgG. Data shown are mean ± SD of percent input DNA, from 3 independent experiments. B, mapping FOXP3 responsive element to 1.5 kb 5′ of transcription start site. The constructs used are diagrammed on the top, whereas the transcriptional activity in the presence or absence of FOXP3 is presented in the bottom. Data shown are mean ± SD of 3 independent analyses. C, identification of FOXP3 responsive element by mutational analysis. Three forkhead binding motifs in P4 were deleted individually and the mutant constructs were tested for their response to FOXP3. Data shown are mean ± SD of 3 independent analyses.

significant reduction in both *Lats1* and *Lats2* mRNA. Similar reductions were observed in the mutant prostate tissue (Fig. 1A,bottom). Because the Scurfy mutation cause frameshift and nonsense-mediated decay of mRNA, a significant reduction of *Foxp3* transcript was also observed in the Scurfy mice. Furthermore, because the level of *Lats1* mRNA was 10-fold less than that of *Lats2*, we have focused on regulation of *Lats2* transcription by Foxp3.

When the lysates were compared for Lats2 and Yap proteins, it is clear that the Lats2 protein level was substantially reduced in the *Foxp3*-deficient epithelial cells from mammary and prostate glands (Fig. 1B). Correspondingly, a selective reduction in phosphorylated Yap was observed (Fig. 1B). We also carried out immunohistochemical analysis of both benign and cancerous tissue from the $Rag2^{-/-}$ and $Rag2^{-/-}$ $Foxp3^{sf/sf}$ mice. As shown in Figure 1C, Lats2 protein was barely detective in the epithelial cells from the $Foxp3^{sf/sf}$ mice and completely absent from $Foxp3^{sf/sf}$ tumors. Consistent with tumor suppressor activity, the spontaneous mammary tumors were observed in the $Rag2^{-/-}Foxp3^{sf/sf}$ but not in the $Rag2^{-/-}Foxp3^{+/+}$ mice (data not shown). Consistent with a role for *Foxp3* in *Lats2* expression, *Foxp3* knockdown in murine mammary tumor cell line TSA (18) leads to reduction of *lats2* transcripts and protein (Fig. 1D).

To study the role for FOXP3 in *LATS2* expression in human cells, we tested the effect of *FOXP3* silencing on immortalized human epithelial cell line MCF10A (19). As shown in Figure 2A, shRNA silencing of *FOXP3* caused a major reduction of *LATS2*

Published OnlineFirst January 28, 2011; DOI:10.1158/0008-5472.CAN-10-3268

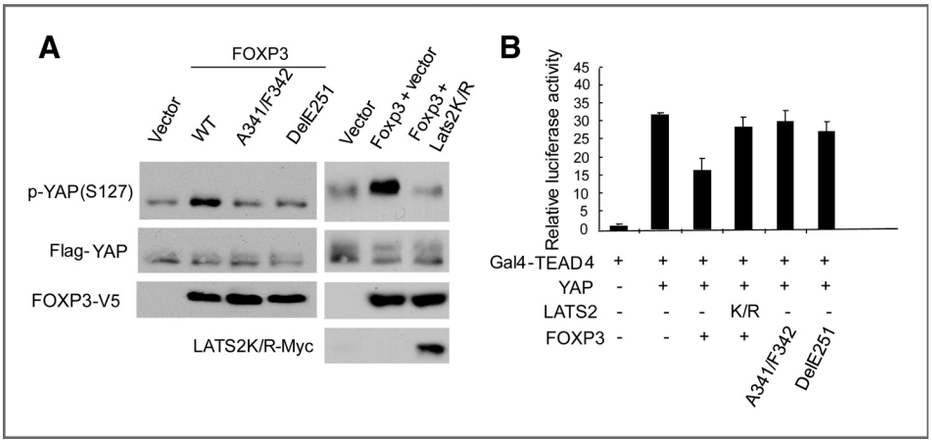

Figure 4. FOXP3 regulates phosphorylation (A) and transcriptional coactivator function of YAP (B): requirement for DNA binding and dimerization of FOXP3 and endogenous LATS. A, mutational analyses suggest the requirement for FOXP3-mediated transcription of *LATS* in FOXP3-induced YAP phosphorylation. Left, the impact of FOXP3 mutations; right, the effect of dominant negative LATS2. 293T cells were transfected with either WT or mutant *FOXP3* cDNA in conjunction with either vector alone or dominant negative mutant of LATS2. At 48 hours after transfection, the transfectants were starved for 8 hours and then lysed for Western blots with antibodies specific for YAP, p-YAP, V5-tag, or Myc-tag. B, FOXP3 inhibited YAP activity. TEAD4 luciferase reporter assay was used to measure coactivation by TEAD4 and YAP. WT or mutant FOXP3 were transfected in conjunction with YAP and Gal4-TEAD4 and 5X UAS-luciferase reporter into 293 T cells. TEAD4 luciferase activity was measured and normalized to renila activity. Data shown are mean ± SD from 3 independent experiments.

transcript (Fig. 2A). As a complementary approach, we used a Tet-off system to test the effect of inducible expression of *FOXP3* on *LATS2* transcripts in the human breast cancer cell line MCF7. As shown in Figure 2B, induction of *FOXP3* progressively increased *LATS2* transcripts. The increase reached more than 10-fold at day 3 in the MCF-7 cells.

To determine whether FOXP3 contribute to *LATS2* expression in the primary tumor samples, we used immunohistochemistry to test whether LATS2 expression correlates with that of nuclear FOXP3. As shown in Supplementary Table S2, 71% of nuclear $FOXP3^+$ tumor samples expressed detectable LATS2, whereas only 46% of $FOXP3^-$ samples expressed detectable LATS2. Chi-square analysis indicated a statistically significant correlation between LATS2 and nuclear FOXP3 expression.

FOXP3 binding to the *LATS2* promoter is essential for LATS2 transcription

We searched the 5′ sequence of the *LATS2* gene for FOXP3 recognition motifs (Forkhead binding motif 5′-RYMAAYA or 3′-YRKTTRT; R = A, G; Y = C, T; M = A, C; K = G, T). The potential binding motifs in *LATS2* promoter were diagramed in Figure 3A (top). We used real-time PCR to determine the amounts of specific DNA sequence in chromatin immunoprecipitates of anti-FOXP3 mAb. The MCF7 tumor cells with induced FOXP3 expression were used as source of chromatin. As shown in Figure 3A, of the 8 regions analyzed, all but one (B3) showed specific binding to FOXP3. To identify a functional element for FOXP3-mediated regulation of LATS2, we generated luciferase reporters consisting of 4 overlapping DNA fragments that cover all of the forkhead binding motifs and tested the effect of FOXP3 on the reporters. As shown in Figure 3B, *FOXP3* cDNA strongly stimulated all 4 regions of the *LATS2* promoter. Although the stimulation of P4 seemed less robust in this experiment, multiple experiments did not support the reduced promoter activity of this region. Therefore, P4 likely contained all necessary FOXP3 responsive *cis* element. To identify the FOXP3 responsive element in the P4, we deleted 3 FOXP3 binding sites in the region, one at a time, and tested their response to *FOXP3* cDNA. As shown in Figure 3C, whereas mutation of B6 and B7 had no effect on response to FOXP3, that of B8 eliminated FOXP3 response of the *LATS2* promoter. Therefore, B8 is the essential FOXP3 response element in the *LATS2* promoter.

FOXP3 activation of the Hippo pathway in normal mouse and human mammary epithelial cells

YAP is the effector molecule repressed by the Hippo pathway and is a coactivator in gene transcription. Although LATS-phosphorylated YAP will be degraded (7), unphosphorylated YAP will translocate into nuclear to form complex with TEAD1-4 to activate gene transcription (20). To test regulation of YAP phosphorylation by FOXP3, we transfected wild-type (WT) or mutant FOXP3 cDNA in conjunction with YAP into 293T cells. Two days after transfection, YAP phosphorylation was determined by immunoblot. As shown in Figure 4A, FOXP3 increased YAP phosphorylation as revealed by antibody specific for phosphor-S127 and by electrophoresis mobility (Figure 4A, right). Mutations that either prevent FOXP3 dimerization (delta252E; ref. 21) or DNA binding (A341F342; ref. 22) abrogated this effect. These data suggest that FOXP3 regulates YAP phosphorylation through its role in gene regulation. Further, the impact of FOXP3 is achieved through LATS as the LATS2 kinase dead mutant (LATS2-K/R), which was known as a dominant negative inhibitor of *LATS* (7), abrogated YAP phosphorylation. We used a reporter system consisting of a 5x UAS-luciferase reporter and a Gal4 DNA binding domain fused to

Published OnlineFirst January 28, 2011; DOI:10.1158/0008-5472.CAN-10-3268

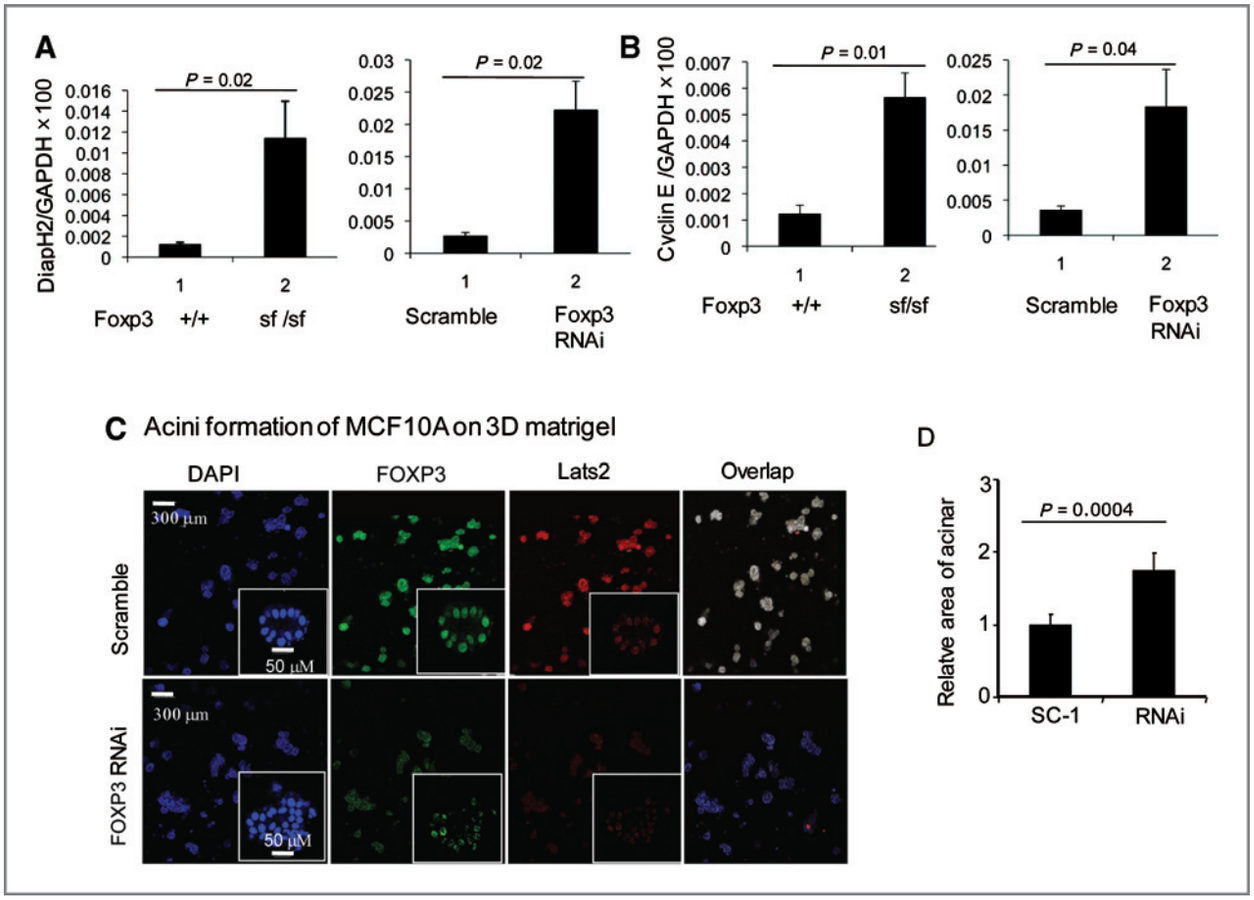

Figure 5. FOXP3 regulates YAP target gene *CYCLINE1* and *DIAPH2* in normal mammary epithelial cells of mouse and human origin and inhibits the growth of human mammary epithelial cells in 3-D culture. A and B, left, quantitation of Diaph2 and Cyclin E2 transcripts of *ex vivo* mammary epithelial cells isolated from $Rag2^{-/-}FoxP3^{+/+}$ and $Rag2^{-/-}FoxP3^{sf/sf}$ mice by real-time PCR. A and B, right, expression of *CYCLINE1* and *DIAPH2* mRNA in MCF10A cells transfected with either scrambled or *FOXP3* shRNA. Transfectants were selected by puromycin for 2 weeks. Stable clones were cultured for RNA analysis. Data shown in A and B are mean ± SD from 3 independent experiments. C, impact of *FOXP3* silencing on acinar formation in MCF10A. MCF10A cell lines transduced with lentiviral vectors control or shRNA were cultured in matrigel medium. Low-power (×10) images of acinar sizes (4′,6-diamidino-2-phenylindole, DAPI) and expression of FOXP3 (green) and LATS2. High-power (×60) images of acinar structure and FOXP3 and LATS2 expression were shown in right corner of each picture. D, measurement of acinar size. The sizes were shown by relative area, measured at 14 days after culture. Data shown are mean ± SD of relative sizes. The mean sizes of the scrambled samples were artificially defined as 1.0.

Tead4(Gal4-Tead4) to test the effect of FOXP3 on coactivator activity of YAP. As showed in Figure 4B, without *YAP* cDNA, Gal4-Tead4 showed very low basal activity. With YAP coexpression, *Gal4-Tead4* reporter was strongly activated. Transfection of FOXP3 reduced reporter activity. Again, the inhibition of the YAP activity is likely mediated by LATS as the LATS2 kinase dead mutant (LATS2-K/R) abrogated FOXP3 function.

CyclinE and *Diaph2* are two well known YAP targets (20). To determine whether *Foxp3* regulates Yap function *in vivo*, we isolated mammary epithelial cells from $Rag2^{-/-}Foxp3^{+/+}$ and $Rag2^{-/-}Foxp3^{sf/sf}$. As shown in Figure 5A and B (left), inactivating mutation of *Foxp3* increased expression of both *CyclinE* and *Diaph2*. Likewise, silencing *FOXP3* in human epithelial cell line MCF10A also increased *CYCLINE* and *DIAPH2* gene expression (Fig. 5A and B, right). In 3-dimensional (3-D) culture, we observed that FOXP3 silencing in the MCF10A cells decreased LATS2 protein levels (Fig. 5C), increased acinar size (Fig. 5D), and increased the number of acini with multiple layers of epithelial cells (Fig. 5C). These phenotypes are consistent with a YAP activation in the cells when FOXP3 is downregulated.

FOXP3–LATS2 interaction contributes to tumor suppression

An important issue is whether *FoxP3*-mediated *Lats2* expression contributes to tumor suppressor function of *Foxp3*. To address this issue, we tested whether the dominant-negative mutant of *Lats2* abrogated tumor suppressor activity. As shown in Figure 6A, *Foxp3* significantly inhibited the growth of murine mammary tumor cell lines TSA *in vitro*, as we had previously reported. This inhibition seemed to require *Foxp3* dimerization and DNA binding, as the inactive *Foxp3* mutants failed to suppress growth of TSA *in vitro*. Importantly, the

Published OnlineFirst January 28, 2011; DOI:10.1158/0008-5472.CAN-10-3268

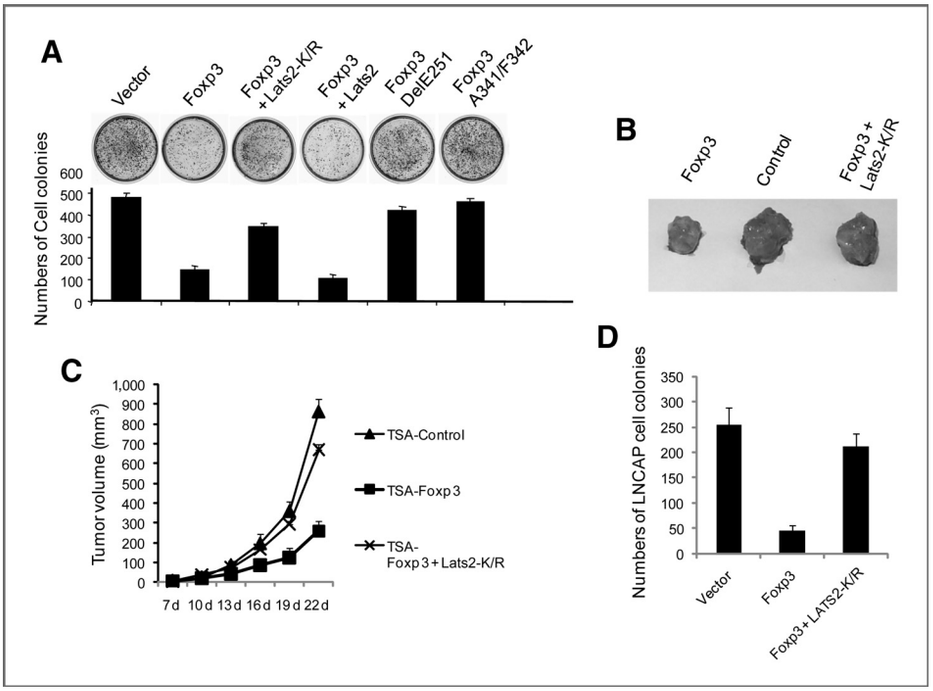

Figure 6. Foxp3-mediated growth inhibition of TSA is at least partially dependent on its regulation of *Lats2*. A, *in vitro* colony formation assay. TSA cells were transfected with indicated plasmid DNA. After drug selection for 10 days, cells were stained with coomassie blue solution and then cell colonies were counted. Representative images are shown at the top, whereas the mean ± SD of colony numbers is shown in the bottom. Data shown are triplicate samples and have been repeated 3 times. B and C, Foxp3–*Lats2* interaction contributes to tumor suppression. TSA cell lines with stable transfection of vector control, Foxp3, or Foxp3 in conjunction with dominant negative mutant of *Lats2* were transplanted into the mammary fat pad of syngeneic BALB/c mice. The tumor sizes were monitored over a 3-week period. B, photograph of a representative tumor from each group, at 25 days after transplantation. C, kinetics of tumor growth. Data shown are mean ± SD and have been repeated 3 times. D, *in vitro* colony formation assay in prostate cancer cell line. Prostate cancer cell line LNCAP was transfected with indicated plasmid DNA. After drug selection for approximately 2 weeks, Cells were stained with coomassie blue solution and then cell colonies were counted. The mean ± SD of colony numbers is presented.

kinase dead mutant of the Lats2 substantially diminished tumor suppressor function of Foxp3.

The growth inhibition pattern was largely recapitulated when the tumor cells were inoculated into the mammary fat pad. A typical example is presented in Figure 6B and the growth kinetics of TSA transfected with vector alone, Foxp3 or Foxp3 + Lats2-K/R mutant is shown in Figure 6C. These data show that growth inhibitory function of FOXP3 is attenuated by Lats2-K/R. To test whether FOXP3 inhibits cell growth in prostate cancer cells, a prostate cancer cell line LNCAP was transfected with FOXP3 alone or FOXP3 plus LATS2 kinase dead mutant LATS2-K/R. The results showed that LATS2-K/R mutant reversed the inhibition of FOXP3 on LNCAP cell growth, thus implying LATS2 as a downstream target for FOXP3-mediated growth inhibition.

FOXP3 defects contribute to *Hippo* inactivation in human prostate cancer

We have recently reported overexpression of YAP protein (7) and downregulation of nuclear FOXP3 proteins (13) in prostate cancer samples. To determine whether FOXP3 downregulation contributes to defective *Hippo* pathway in prostate cancer, we analyzed expression of *LATS2*, *YAP*, and *FOXP3* mRNA in microdissected samples. Much like *FOXP3* transcripts, *LATS*2 is downregulated in overwhelming majority of microdissected cancer cells, in comparison with normal prostate epithelial from the same patients (Fig. 7A, top). Moreover, we have recently uncovered 4 of 20 samples that harbor somatic *FOXP3* missense mutations (13). As shown in Figure 7A (bottom), in each of the 4 cases, the tumor samples show greatly reduced *LATS2* levels. Interestingly, downregulation of *LATS2* strongly correlates with that of *FOXP3* (Fig. 7B, top). In contrast, the levels of *YAP* transcripts show no correlation to that of FOXP3 ($r^2 < 0.5$; Fig. 7B, bottom). Therefore, *FOXP3* defects are likely a major determinant of *LATS2* levels in prostate cancer. Because either overexpression of *YAP* or downregulation of *LATS2* can lead to activation of the *hippo* pathway, we plotted the mRNA levels of *YAP* and *Lats* of the 20 microdissected tumor samples. As shown in Figure 7C, the two genes seemed to be independently regulated.

A major indication of Hippo activation is accumulation of YAP protein in the nuclei. Although the cohort is too small to compare the relative importance of the two events, we were interested in whether downregulation of *LATS2* could lead to nuclear accumulation of YAP in samples that showed no or little upregulation of *YAP* mRNA. We tested 3 cases of prostate cancer samples in which YAP expression is not significantly

Published OnlineFirst January 28, 2011; DOI:10.1158/0008-5472.CAN-10-3268

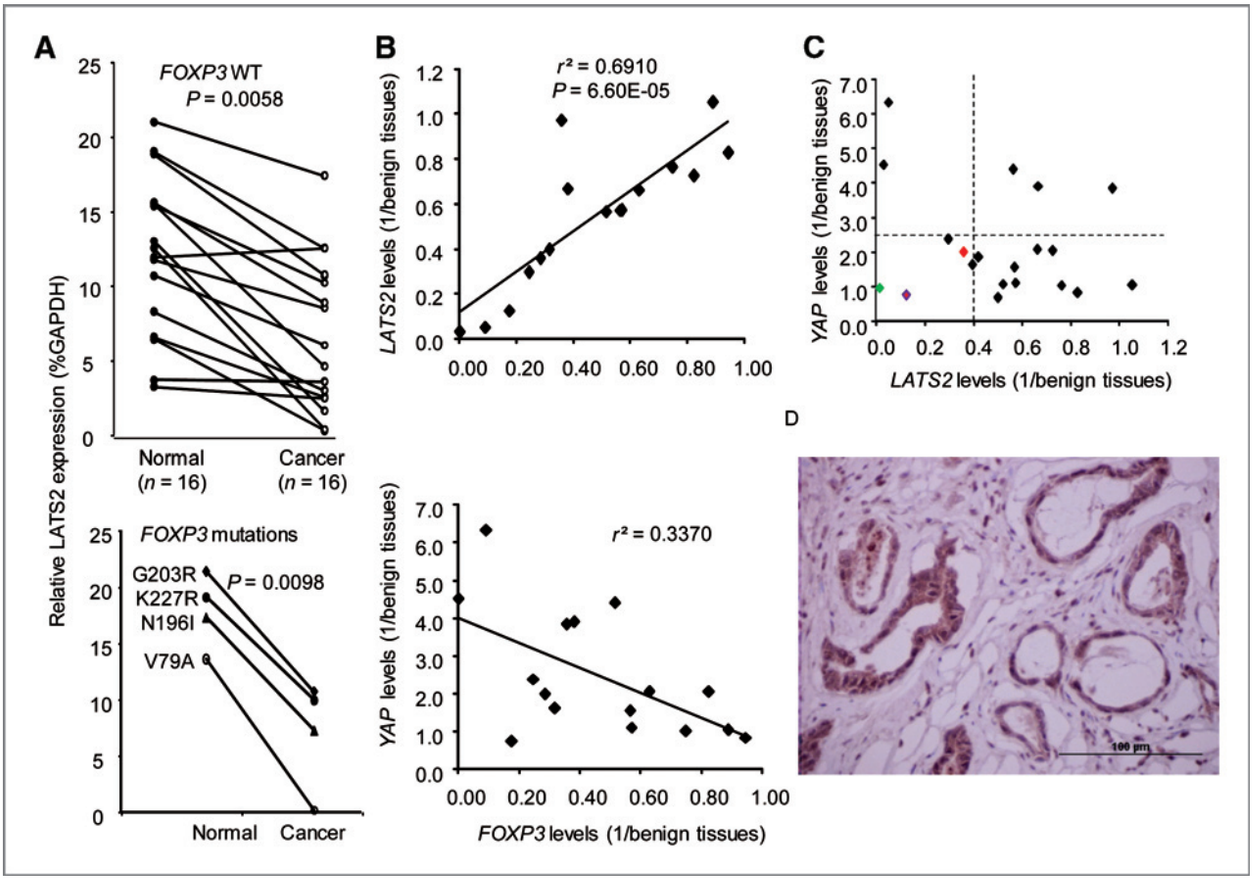

Figure 7. *FOXP3* defects contribute to *LATS2* mRNA downregulation and increased YAP protein level in human prostate cancer samples. A, downregulation of *LATS2* mRNA in prostate cancer tissues in comparison with normal tissues from the same patients. The samples were isolated by laser-guided microdissections. Data from samples with no somatic missense mutation of FOXP3 were shown in the top, whereas those with missense mutations are shown in the bottom. *P* values were calculated by Wilcox 2-sample tests. B, correlations between downregulations of *FOXP3* and *LATS2* mRNA (top) or between *FOXP3* and *YAP* mRNA (bottom). Only those with no missense mutation of the *FOXP3* gene are presented. Data shown are ratios of transcript levels of cancer samples over benign tissues from the same patients. *P* values by Mann–Whitney *U* test. C, independent regulation of *YAP* and *LATS2* mRNA in prostate cancer tissue. The ratio of the mRNA levels in microdissected cancer over benign epithelial tissue from prostate cancer patients was presented; quadroons show boundary of 2.5-fold increases of *YAP* and 2.5-fold decreases of *LATS2* transcripts. The red, green, and purple dots indicate samples that were confirmed to have accumulation of nuclear YAP proteins. D, accumulation of nuclear YAP in prostate cancer samples with no increase in *YAP* transcripts. The data shown are representative of 3 samples in the group; the relative level of LATS2 and YAP mRNA in this sample is shown in C (purple dot).

elevated (red, green, and purple dots in Fig. 7C). In all 3 cases, clear accumulation of nuclear YAP was observed (see Fig. 7D for an example).

It is possible that the increase of nuclear YAP is caused by mutation of the LATS2 phosphorylation sites (S127 and S347). To address this possibility, we carried out sequence analysis of exons 2 and 6 (which encodes part of YAP that contains S127 and S347, respectively) of the *YAP* gene in microdissected samples. Our data revealed that none of the 20 cancer samples tested had mutation in the 2 exons. Because *FOXP3* defects correlated with decreased *LATS2* expression, and because *LATS2* downregulation correlated with increased YAP protein in the absence of either activating *YAP* mutation or overexpression, it is likely that FOXP3 defects is a cause of YAP activation in the prostate cancer.

Discussion

FOXP3 is an X-linked tumor suppressor gene for breast and prostate cancers (13, 14, 23). As a transcription factor, FOXP3 has been shown to both downregulate oncogenes, including *ERBB2* (14), *SKP2* (15), and *cMYC* (13) and upregulate tumor suppressors such as *p21* (16). Here we showed a tumor suppressor relay between the *FOXP3* and *Hippo* pathways.

Our data show that FOXP3 directly interacts with the *LATS2* promoter region to enhance the expression of *LATS2* gene. The induction of *LATS2* caused increased phosphorylation and reduction of total levels of oncoprotein YAP. Using a dominant-negative *LATS2* mutant, we showed a critical role for the *FOXP3–LATS2* regulation in tumor suppressor function of FOXP3. The cross-regulation has been shown in both normal and malignant cells in mouse and human. These data not only

Published OnlineFirst January 28, 2011; DOI:10.1158/0008-5472.CAN-10-3268

further elucidate the mechanism of FOXP3-mediated tumor suppression but also broaden the impact of FOXP3 in pathogenesis of both breast and prostate cancer.

The *FOXP3–LATS2* connection may contribute to the frequent loss of LATS2 transcripts and protein in breast (9) and prostate (10) cancers as high frequency of cancer sampled show mutation, deletion, and/or abnormal expression of FOXP3 (13–15, 24). The strong correlation between downregulation (or mutations) of *FOXP3* and *LATS2* expression, as shown here with microdissected prostate cancer samples, indicate that, at least for prostate cancer, defects in FOXP3 are likely a major mechanism for *LATS2* loss. Our data from breast cancer TMA samples also show a significant correlation between loss of nuclear FOXP3 protein and LATS2 protein in cancer cells. However, the correlation is less striking than the prostate cancer samples. This variance in degree of correlations in the 2 cancers may be caused by the higher sensitivity and accuracy of real-time PCR analysis of microdissected samples than immunohistochemistry of TMA samples. Alternatively, it is also possible that the relative importance of FOXP3 defects in LATS2 downregulation differs in the 2 cancer types.

It is well documented that YAP protein is frequently upregulated in human cancer, including prostate (7), breast (25), colon (25), ovary (25), lung (25, 26), and liver (7, 27) cancers. At least 3 mechanisms can be involved in the elevation of the YAP protein. First, YAP gene resides in 11q22, which is amplified in significant numbers of cancer samples (28). This amplification can naturally lead to increased YAP expression. In our microdissected prostate cancer samples, we observed 2.5-fold or more increase in YAP transcript in approximately 25% of cancer samples. This upregulation does not correlate with reduced FOXP3 expression and may be due to gene amplification or other mechanisms. Second, downregulation of *LATS2* may be involved in YAP upregulation as LATS2-mediated phosphorylation targets YAP for degradation (6, 7). Because LATS2 downregulation strongly associates with FOXP3 downregulation in prostate and breast cancers, FOXP3 defects may contribute to YAP upregulation. Thirdly, mutation of YAP phosphorylation sites that target it for degradation could result in YAP accumulation. However, our sequencing of YAP gene of 20 prostate cancer samples revealed no somatic mutation in the exon encoding the phosphorylation sites. Therefore, *YAP* mutation is unlikely a major cause of YAP protein upregulation in prostate cancer.

Disclosure of Potential Conflicts of Interest

No potential conflicts of interest were disclosed.

Acknowledgment

We thank Dr. Kun-Liang Guan for valuable discussions, reagents, and critical reading of the manuscript and Ms. Darla Kroft for editorial assistance.

Grant Support

This study is supported by the NIH and Department of Defense.

The costs of publication of this article were defrayed in part by the payment of page charges. This article must therefore be hereby marked *advertisement* in accordance with 18 U.S.C. Section 1734 solely to indicate this fact.

Received September 7, 2010; revised December 7, 2010; accepted December 30, 2010; published OnlineFirst January 28, 2011.

References

1. Harvey K, Tapon N. The Salvador-Warts-Hippo pathway – an emerging tumour-suppressor network. Nat Rev Cancer 2007;7:182–91.
2. O'Neill E, Kolch W. Taming the Hippo: Raf-1 controls apoptosis by suppressing MST2/Hippo. Cell Cycle 2005;4:365–7.
3. Pan D. Hippo signaling in organ size control. Genes Dev 2007;21:886–97.
4. St John MA, Tao W, Fei X, Fukumoto R, Carcangiu ML, Brownstein DG, et al. Mice deficient of Lats1 develop soft-tissue sarcomas, ovarian tumours and pituitary dysfunction. Nat Genet 1999;21:182–6.
5. McPherson JP, Tamblyn L, Elia A, Migon E, Shehabeldin A, Matysiak-Zablocki E, et al. Lats2/Kpm is required for embryonic development, proliferation control and genomic integrity. EMBO J 2004; 23:3677–88.
6. Dong J, Feldmann G, Huang J, Wu S, Zhang N, Comerford SA, et al. Elucidation of a universal size-control mechanism in Drosophila and mammals. Cell 2007;130:1120–33.
7. Zhao B, Wei X, Li W, Udan RS, Yang Q, Kim J, et al. Inactivation of YAP oncoprotein by the Hippo pathway is involved in cell contact inhibition and tissue growth control. Genes Dev 2007;21:2747–61.
8. Zhao B, Li L, Tumaneng K, Wang CY, Guan KL. A coordinated phosphorylation by Lats and CK1 regulates YAP stability through SCF(beta-TRCP). Genes Dev 2010;24:72–85.
9. Takahashi Y, Miyoshi Y, Takahata C, Irahara N, Taguchi T, Tamaki Y, et al. Down-regulation of LATS1 and LATS2 mRNA expression by promoter hypermethylation and its association with biologically aggressive phenotype in human breast cancers. Clin Cancer Res 2005;11:1380–5.
10. Powzaniuk M, McElwee-Witmer S, Vogel RL, Hayami T, Rutledge SJ, Chen F, et al. The LATS2/KPM tumor suppressor is a negative regulator of the androgen receptor. Mol Endocrinol 2004;18:2011–23.
11. Jiang Z, Li X, Hu J, Zhou W, Jiang Y, Li G, et al. Promoter hypermethylation-mediated down-regulation of LATS1 and LATS2 in human astrocytoma. Neurosci Res 2006;56:450–8.
12. Jimenez-Velasco A, Roman-Gomez J, Agirre X, Barrios M, Navarro G, Vazquez I, et al. Downregulation of the large tumor suppressor 2 (LATS2/KPM) gene is associated with poor prognosis in acute lymphoblastic leukemia. Leukemia 2005;19:2347–50.
13. Wang L, Liu R, Li W, Chen C, Katoh H, Chen GY, et al. Somatic single hits inactivate the X-linked tumor suppressor FOXP3 in the prostate. Cancer Cell 2009;16:336–46.
14. Zuo T, Wang L, Morrison C, Chang X, Zhang H, Li W, et al. FOXP3 is an X-linked breast cancer suppressor gene and an important repressor of the HER-2/ErbB2 oncogene. Cell 2007;129:1275–86.
15. Zuo T, Liu R, Zhang H, Chang X, Liu Y, Wang L, et al. FOXP3 is a novel transcriptional repressor for the breast cancer oncogene SKP2. J Clin Invest 2007;117:3765–73.
16. Liu R, Wang L, Chen G, Katoh H, Chen C, Liu Y, et al. FOXP3 up-regulates p21 expression by site-specific inhibition of histone deacetylase 2/histone deacetylase 4 association to the locus. Cancer Res 2009;69:2252–9.
17. Chen GY, Chen C, Wang L, Chang X, Zheng P, Liu Y. Cutting edge: Broad expression of the FoxP3 locus in epithelial cells: a caution against early interpretation of fatal inflammatory diseases following in vivo depletion of FoxP3-expressing cells. J Immunol 2008;180:5163–6.

Published OnlineFirst January 28, 2011; DOI:10.1158/0008-5472.CAN-10-3268

18. Nanni P, de Giovanni C, Lollini PL, Nicoletti G, Prodi G. TS/A: a new metastasizing cell line from a BALB/c spontaneous mammary adenocarcinoma. Clin Exp Metastasis 1983;1:373–80.
19. Soule HD, Maloney TM, Wolman SR, Peterson WD Jr, Brenz R, McGrath CM, et al. Isolation and characterization of a spontaneously immortalized human breast epithelial cell line, MCF-10. Cancer Res 1990;50:6075–86.
20. Zhao B, Ye X, Yu J, Li L, Li W, Li S, et al. TEAD mediates YAP-dependent gene induction and growth control. Genes Dev 2008;22:1962–71.
21. Lopes JE, Torgerson TR, Schubert LA, Anover SD, Ocheltree EL, Ochs HD, et al. Analysis of FOXP3 reveals multiple domains required for its function as a transcriptional repressor. J Immunol 2006;177:3133–42.
22. Wu Y, Borde M, Heissmeyer V, Feuerer M, Lapan AD, Stroud JC, et al. FOXP3 controls regulatory T cell function through cooperation with NFAT. Cell 2006;126:375–87.
23. Liu Y, Wang L, Zheng P. X-linked tumor suppressors: perplexing inheritance, a unique therapeutic opportunity. Trends Genet 2010;26:260–5.
24. Ladoire S, Arnould L, Mignot G, Coudert B, Rebe C, Chalmin F, et al. Presence of Foxp3 expression in tumor cells predicts better survival in HER2-overexpressing breast cancer patients treated with neoadjuvant chemotherapy. Breast Cancer Res Treat 2010.
25. Steinhardt AA, Gayyed MF, Klein AP, Dong J, Maitra A, Pan D, et al. Expression of Yes-associated protein in common solid tumors. Hum Pathol 2008;39:1582–9.
26. Wang Y, Dong Q, Zhang Q, Li Z, Wang E, Qiu X. Overexpression of yes-associated protein contributes to progression and poor prognosis of non-small-cell lung cancer. Cancer Sci 2010;101:1279–85.
27. Xu MZ, Yao TJ, Lee NP, Ng IO, Chan YT, Zender L, et al. Yes-associated protein is an independent prognostic marker in hepatocellular carcinoma. Cancer 2009;115:4576–85.
28. Dai Z, Zhu WG, Morrison CD, Brena RM, Smiraglia DJ, Raval A, et al. A comprehensive search for DNA amplification in lung cancer identifies inhibitors of apoptosis cIAP1 and cIAP2 as candidate oncogenes. Hum Mol Genet 2003;12:791–801.

Molecular Cell
Article

FOXP3 Orchestrates H4K16 Acetylation and H3K4 Trimethylation for Activation of Multiple Genes by Recruiting MOF and Causing Displacement of PLU-1

Hiroto Katoh,[1] Zhaohui S. Qin,[2] Runhua Liu,[1] Lizhong Wang,[1] Weiquan Li,[1] Xiangzhi Li,[3] Lipeng Wu,[3] Zhanwen Du,[6] Robert Lyons,[4,7] Chang-Gong Liu,[8] Xiuping Liu,[8] Yali Dou,[3,4] Pan Zheng,[1,3,*] and Yang Liu[1,3,5,*]
[1]Division of Immunotherapy, Department of Surgery, University of Michigan School of Medicine and Cancer Center, Ann Arbor, MI 48109, USA
[2]Department of Biostatistics and Bioinformatics, Rollins School of Public Health, Center for Comprehensive Informatics, Emory University, Atlanta, GA 30329, USA
[3]Department of Pathology
[4]Department of Biological Chemistry
[5]Department of Internal Medicine
University of Michigan School of Medicine, Ann Arbor, MI 48109, USA
[6]State Key Laboratory for Macromolecules and Key Laboratory of Infection and Immunity, Institute of Biophysics, Chinese Academy of Science, Beijing, China
[7]DNA Sequencing Core, University of Michigan, Ann Arbor, MI 48109, USA
[8]University of Texas M.D. Anderson Medical Center, Houston, Texas, TX 77030, USA
*Correspondence: yangl@med.umich.edu (Y.L.), panz@med.umich.edu (P.Z.)
DOI 10.1016/j.molcel.2011.10.012

SUMMARY

Both H4K16 acetylation and H3K4 trimethylation are required for gene activation. However, it is still largely unclear how these modifications are orchestrated by transcriptional factors. Here, we analyzed the mechanism of the transcriptional activation by FOXP3, an X-linked suppressor of autoimmune diseases and cancers. FOXP3 binds near transcriptional start sites of its target genes. By recruiting MOF and displacing histone H3K4 demethylase PLU-1, FOXP3 increases both H4K16 acetylation and H3K4 trimethylation at the FOXP3-associated chromatins of multiple FOXP3-activated genes. RNAi-mediated silencing of *MOF* reduced both gene activation and tumor suppression by FOXP3, while both somatic mutations in clinical cancer samples and targeted mutation of FOXP3 in mouse prostate epithelial cells disrupted nuclear localization of MOF. Our data demonstrate a pull-push model in which a single transcription factor orchestrates two epigenetic alterations necessary for gene activation and provide a mechanism for somatic inactivation of the FOXP3 protein function in cancer cells.

INTRODUCTION

FOXP3 was initially identified by severe autoimmune diseases associated with its mutations in mouse and human (Bennett et al., 2001; Brunkow et al., 2001; Chatila et al., 2000; Hori et al., 2003; Wildin et al., 2001), and has emerged as a key transcriptional regulator for the development and function of regulatory T cells (Treg) (Fontenot et al., 2003; Hori et al., 2003). Recently *FOXP3* has emerged as an important X-linked tumor suppressor for breast and prostate cancers, as it is somatically inactivated in both prostate and breast cancer samples (Liu et al., 2010; Wang et al., 2009a; Zuo et al., 2007b). A spontaneous germline mutation of *Foxp3* in female mice resulted in significantly increased incidences of mammary carcinoma (Zuo et al., 2007b), while prostate-specific deletion of *Foxp3* caused prostatic hyperplasia and prostatic intraepithelial neoplasm (Wang et al., 2009a). As a transcription factor, FOXP3 directly regulates transcription of important cancer-related genes such as *ERBB2* (*Her2/neu*) (Zuo et al., 2007b), *c-MYC* (Wang et al., 2009a), *SKP2* (Zuo et al., 2007a), and *p21* (Liu et al., 2009). However, how FOXP3 regulates gene expression is largely unclear.

Dynamic histone modifications play a pivotal role in the regulation of gene transcription (Strahl and Allis, 2000). A subset of specific histone modification results in chromatin condensation (inactive state for transcription), while other subsets of histone modifications facilitate chromatin decondensation (active state for transcription). Within the eukaryotic genome, actively transcribed euchromatin is marked with acetyl-H3 and acetyl-H4 and trimethylation of H3K4 (H3K4me3), while transcriptionally inactive heterochromatin exhibits hypoacetylation of H3 and H4 and trimethylation of H3K27 (H3K27me3) and K9 (H3K9me3) and H4K20 (H4K20me3) (Lee and Workman, 2007; Martin and Zhang, 2005). Among lysine residues on histone H4, acetylation of H4K16 (H4K16ac) is thought to be a founder event of H4 acetylation and plays an important role in active transcription, presumably by facilitating chromatin decondensation (Dion et al., 2005; Robinson et al., 2008; Shogren-Knaak et al., 2006). H3K4me3, occurring at transcription start sites (TSS), is also correlated with active transcription (Martin and Zhang,

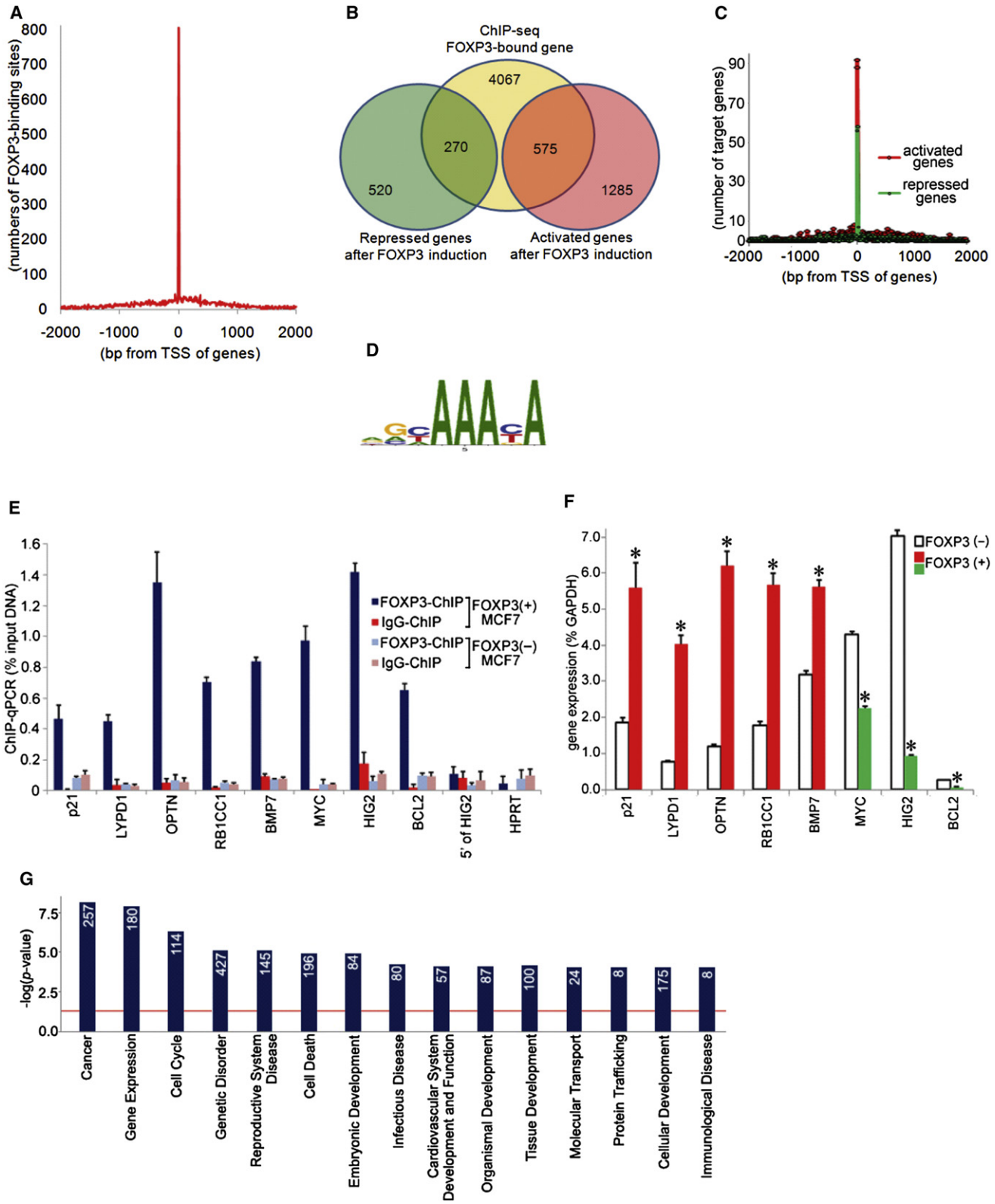

Figure 1. FOXP3-ChIP-Seq Analysis Identified Direct Target Genes of FOXP3 in MCF7 Cells

(A) Distribution of FOXP3-binding sites revealed by ChIP-seq in relation to TSS of genes. The x axis represents the distance between ChIP-peaks and TSSs of genes; the y axis indicates the number of binding sites.

2005; Wang et al., 2009b). These histone modifications are regulated by a variety of enzymes. MOF is a MYST family histone acetyltransferase and specifically acetylates histone H4K16 (Dou et al., 2005; Smith et al., 2005; Taipale et al., 2005). Likewise, methylation of H3K4 is positively regulated by Set domain-containing histone methyltransferases, such as MLL/SET1 family members (MLL1-4 and hSET1), and negatively regulated by histone demethylases, such as JARID family members (e.g., PLU-1) and as yet unidentified enzymes (Martin and Zhang, 2005; Mosammaparast and Shi, 2010; Shi and Whetstine, 2007). MOF and MLL1 work in concert to activate the *HOX* gene by facilitating both H4K16ac and H3K4me3 at the promoter (Dou et al., 2005). However, how these two enzymes are recruited to specific loci by transcription factors is largely unknown.

Dysregulations of histone modifications are important hallmarks of cancer cells (Chi et al., 2010). Significant downregulations of H4K16ac and H4K20me3 in the global genome were observed in various cancers (Fraga et al., 2005). Multiple histone modification enzymes, such as JARID1C, PLU-1, LSD1, SETD2, UTX, EZH2, and MOF, are aberrantly expressed or somatically mutated in cancers (Dalgliesh et al., 2010; Duns et al., 2010; Kleer et al., 2003; Lu et al., 2010; Pfister et al., 2008; Yamane et al., 2007). Moreover, HDAC inhibitors have shown promising effects in cancer therapy (Minucci and Pelicci, 2006). These data suggest that improper histone modifications play an important role in the molecular pathogenesis of cancers.

Since FOXP3 changes various histone modifications, including H3K27me3, H3K4me3, and acetylation of H3 and H4 at binding loci (Pan et al., 2009; Zheng et al., 2007), it is plausible that FOXP3 works in concert with histone modification enzymes to exert its function as a transcription factor. Supporting this hypothesis, recent studies revealed that FOXP3 interacts with histone acetyltransferase TIP60, HDACs, and histone modifying complex EOS/CtBP1 on chromatin to repress its target genes (Li et al., 2007; Pan et al., 2009). While Foxp3 appears to increase H3K4me3 levels at its binding sites in T cells (Zheng et al., 2007), a general mechanism of FOXP3-mediated gene activation remains elusive. In breast cancer cells, FOXP3 increases H3 acetylation by removing HDAC2 and HDAC4 from its binding site at the *p21* locus (Liu et al., 2009).

We carried out chromatin-immunoprecipitation followed by next-generation sequencing (ChIP-seq) to identify FOXP3-binding sites in breast cancer cells. In combination with microarray analysis, we identified at least 845 direct targets. FOXP3-mediated gene activation correlated with both H4K16ac and H3K4me3. For multiple FOXP3 target genes, these crucial epigenetic modifications are simultaneously achieved by recruiting MOF and by displacing an H3K4 demethylase PLU-1. Our data suggest a pull-push model for gene activation by transcription factors.

RESULTS

Characterization of FOXP3-Binding Sites in Breast Cancer Cells

As a source of chromatin for ChIP-Seq, we induced FOXP3 in MCF7 human breast cancer cells with a FOXP3-tet-off system (Zuo et al., 2007b). The DNA precipitated by control-IgG was used as a control. Remarkably, FOXP3 binding was highly focused to regions less than 100 bp of TSS (Figure 1A). We combined the ChIP-seq result with our previous gene expression analysis of FOXP3-induced MCF7 cells (MIAExpress; E-MTAB-73) (Liu et al., 2009). As analyzed in Figure S1, FOXP3-binding sites of putative direct targets were most frequently located within 1 kb of TSS and, when the accumulating events were considered, most of the FOXP3-binding sites reside within 2 kb of TSS. Therefore, we defined direct target genes according to the following criteria: (1) genes with FOXP3 binding within 2 kb of their TSS, and (2) genes whose mRNA expressions in FOXP3-induced cells were >150% or <66% of those in control cells (Liu et al., 2009). Among a total of 4,067 genes that have FOXP3-binding sites within 2 kb of their TSS (Figure 1B), we identified 845 direct target genes, in which 270 and 575 genes were repressed and activated by FOXP3, respectively (Figure 1B and Tables S1 and S2). Importantly, FOXP3-binding sites of these direct targets were also highly enriched around their TSS, although the distribution is slightly broader than the total pool of FOXP3-bound genes (Figure 1C). A known forkhead DNA motif was significantly enriched among the FOXP3-binding sites (Figure 1D and Table S3), which indicated the robustness of our ChIP-seq analysis. The specific interactions of FOXP3 and the effects on gene expression were validated by ChIP-qPCR and RT-qPCR (Figures 1E and 1F), respectively. Gene ontology analysis revealed that FOXP3's direct targets were significantly enriched for genes related to cancer biology, cell cycles, cell death, and cellular development (Figure 1G). Since normal epithelial cells expressed less FOXP3 than what was used for

(B) ChIP-seq identified 4067 genes that were directly bound by FOXP3 between −2 kbp and +2 kbp from their TSSs in MCF7 cells, among which 270 were downregulated, while 575 were upregulated by FOXP3 (genes are listed in Tables S1 and S2).
(C) Distribution of FOXP3-binding sites among direct targets of FOXP3 in relation to TSS. The activated genes are depicted in red, while the repressed genes are shown in green.
(D) A known forkhead DNA binding motif that was enriched among FOXP3-binding sites with a statistical significance (overrepresentation = 2.17, Z score = 5.38; see Table S3).
(E) ChIP-qPCR of target genes of FOXP3 using MCF7 cells with and without FOXP3 induction. Means of triplicate qPCR reactions are shown and error bars represent +1 SD. The y axis represents percentage of input DNA. *HPRT* gene locus and 5′-upstream of the *HIG2* gene were used as negative controls.
(F) mRNA levels of target genes of FOXP3. qRT-PCR was performed to examine mRNA expression levels of FOXP3's target genes before and after FOXP3 induction. Error bars in (E) and (F) represent +1 SD of triplicate qPCR. *: $p < 0.05$ (t test).
(G) Functional categories of the direct target genes of FOXP3. Enrichment of functional categories among FOXP3's direct target genes (listed in Tables S1 and S2) were calculated by Ingenuity Pathway Analysis software (http://www.ingenuity.com) and by comparing them with those among randomly pooled human genes in the software. The y axis represents –log(p value)s, and categories ranked within the top 15 smallest p values are listed. Red line: $p = 0.05$. Numbers of genes in each category are indicated as inserts in the bars.

the study, we tested whether, at levels found in normal epithelial cells, FOXP3 also induced a similar spectrum of gene activation. As shown in Figure S2, inducing FOXP3 at levels found in normal breast/prostate epithelial cells also caused broad activation of most of the genes identified when higher levels of FOXP3 were induced, although the magnitude of gene activation is less pronounced. Moreover H4K16ac- and H3K4me3-ChIP on the LYPD1 promoter clearly showed that these histone modifications were also affected by the physiological expression of FOXP3 (Figure S2D). Furthermore, we evaluated the effects of shRNA silencing of *FOXP3* by profiling mRNA expression of putative FOXP3 targets in MCF10A, an immortalized but nontumorigenic breast epithelial cell line. As shown in Figure S2E, 41%–46% of the activated FOXP3 targets in MCF7 cells were significantly downregulated by the FOXP3-knockdown in MCF10A cells. This is significantly higher than either unaffected or upregulated genes ($p < 0.05$). Thus, high proportions of FOXP3 targets identified by our FOXP3-tet-off MCF7 system are physiologically relevant.

Other groups have performed global FOXP3-ChIP analyses using human or mouse Treg cells (Birzele et al., 2011; Marson et al., 2007; Sadlon et al., 2010; Zheng et al., 2007). We compared our ChIP-seq results with those from others (Figure S3). When compared to human FOXP3-ChIP databases, 58.5% (494/845) of the FOXP3 targets genes in MCF7 cells overlapped with either or both of previous databases (Figure S3A). This overlap is considerably greater than other pairwise comparisons. When compared to mouse Foxp3-ChIP databases, only 13.4% (113/845 genes) of our genes were overlapped with previous databases (Figure S3B). However, human Treg FOXP3-ChIP and mouse Treg Foxp3-ChIP also showed only small overlaps (Figure S3C). Likewise, <10% overlaps were observed in two reports of mouse FOXP3 targets (Figure S3C).

FOXP3 Induces H4K16ac on Both Activated and Repressed Target Genes by Recruiting MOF

In Tregs, a subset of histone modifications such as H3K27me3 and acetyl-H3 are known to be correlated with the FOXP3 binding (Pan et al., 2009; Zheng et al., 2007). We confirmed that these histone modifications were also affected by FOXP3 in MCF7 cells (Figure S4). Acetyl-H4 is an important histone mark for gene activation, and a previous study reported that FOXP3 directly or indirectly mediates acetylation of pan-histone H4 in T cells (Pan et al., 2009). Histone H4 has various lysine residues which can be substrates for acetylation and, among them, H4K16ac is a founder event of the H4 acetylation (Dion et al., 2005). In order to investigate whether or not the H4K16ac is correlated with FOXP3-mediated gene activation in MCF7 cells, we compared H4K16ac levels at FOXP3 binding sites before and after FOXP3 induction. Surprisingly, ChIP-qPCR at FOXP3 binding sites of randomly chosen four activated and three repressed promoters demonstrated broad inductions of H4K16ac by FOXP3, regardless of whether the genes were activated or repressed (Figure 2A). To substantiate the broad correlation between FOXP3 binding and H4K16ac, we performed a confocal imaging analysis. As shown in Figures 2B and 2C, FOXP3 and H4K16ac exhibited an almost complete

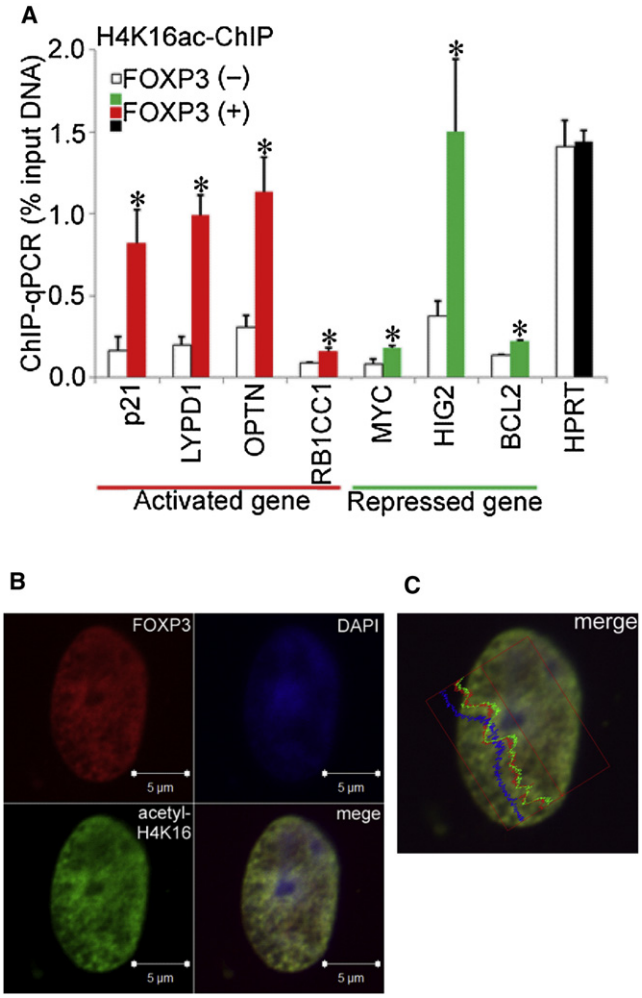

Figure 2. H4K16ac Is Induced by FOXP3 Binding

(A) H4K16ac levels at FOXP3 binding sites were examined by ChIP-qPCR before and after FOXP3 induction in the FOXP3-tet-off MCF7 cell. The y axis represents enrichments of the H4K16ac (percentage of input DNA). Error bars represent +1 SD of triplicate qPCR. *: $p < 0.05$ (t test). n.s.: not significant.

(B) A representative confocal image of FOXP3 (red) and H4K16ac (green) in the MCF7 cell transfected with FOXP3. White bars represent 5 μm. A similar pattern was observed in 10/10 cells analyzed.

(C) A representative signal intensity profile in the confocal image (Figure 2B) is shown. Red, green, and blue graphs indicate signal intensities of FOXP3, H4K16ac, and DAPI, respectively.

overlap throughout the nuclei of the MCF7 cells (Specificity controls are provided in Figure S5). The complete overlap was observed in all cells analyzed (10/10, data not shown).

Since the histone acetyltransferase MOF is both necessary and sufficient for a great majority of H4K16ac in mammals (Li and Dou, 2010), the broad correlation between FOXP3 binding and H4K16ac suggested that FOXP3 may recruit MOF to its binding sites. To test this hypothesis, we performed anti-FLAG-ChIP before and after FOXP3 induction using FLAG-MOF-transfected FOXP3-tet-off MCF7 cells. As shown in Figure 3A, FOXP3 specifically recruited MOF onto FOXP3-binding sites. Confocal microscope analyses revealed virtual overlaps

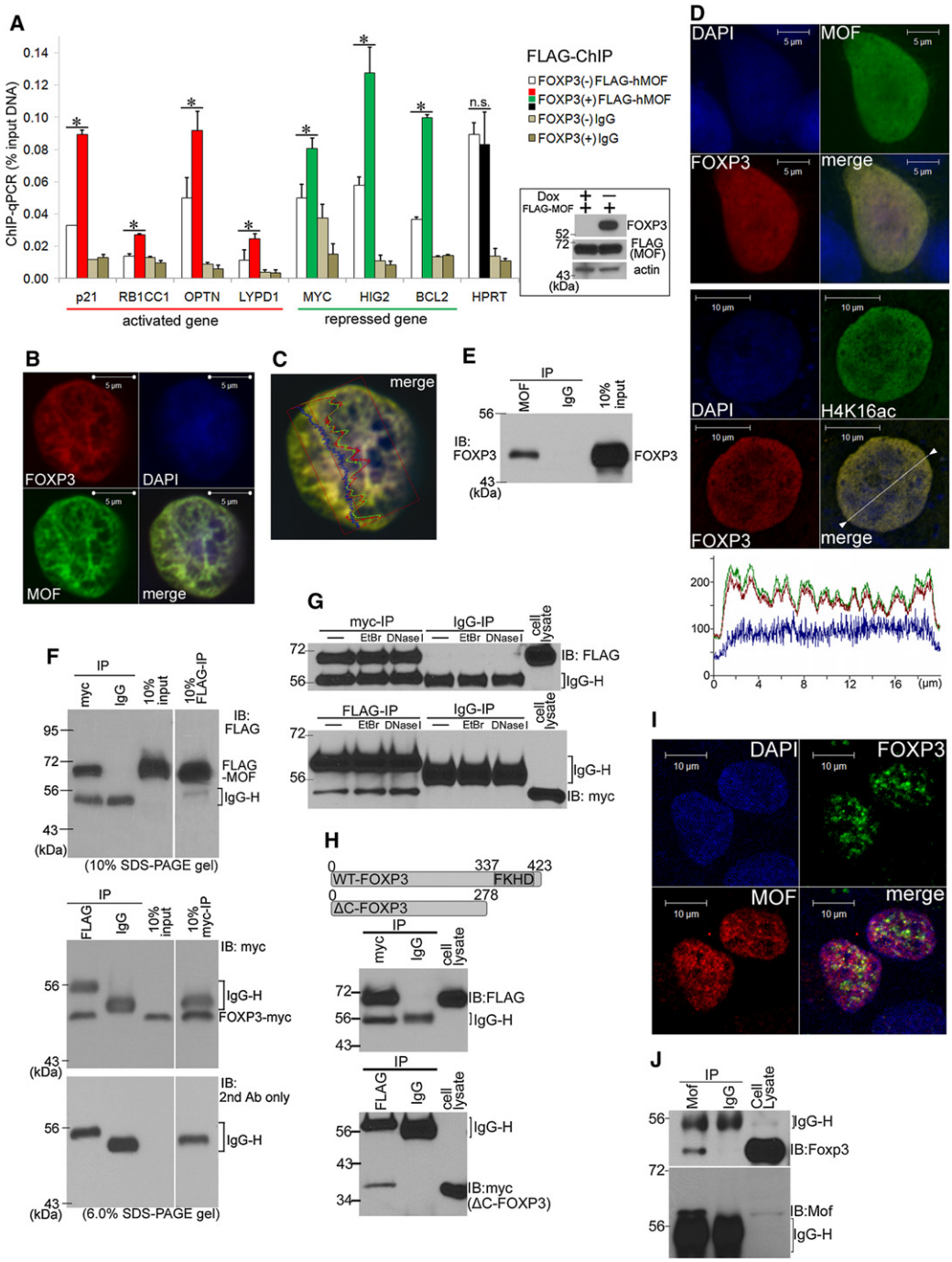

Figure 3. FOXP3 Interacts with MOF at the Chromatin of FOXP3 Target Genes

(A) FLAG-MOF was expressed in FOXP3-tet-off MCF7 cells, and ChIP-qPCR was performed using an anti-FLAG antibody. White and colored (red, green, and black) bars represent percentage of input DNA before and after FOXP3 induction, respectively. Error bars represent +1 SD of triplicate qPCR. *: $p < 0.05$ (t test). n.s.: not significant. Western blots of FOXP3 and MOF are shown in the bottom right panel. DOX: doxycyline.

(B) A representative confocal image of the MCF7 cell transfected with FOXP3 and MOF. FOXP3 (red) and MOF (green) were stained by anti-FOXP3 and anti-MOF antibodies, respectively. Similar patterns were observed in all ten cells analyzed.

(C) A signal intensity profile of the FOXP3 and MOF in the MCF7 cell in Figure 3B is shown. Red, green, and blue graphs indicate signal intensities of FOXP3, MOF, and DAPI, respectively.

(D) Colocalization of MOF, H4K16ac, and FOXP3 on chromatin as revealed by immunofluorescence after in situ subcellular fractionation. Controls are shown in Figure S6. Signal intensity profile of the confocal image is shown in the bottom panel. Red, green, and blue graphs indicate signal intensities of FOXP3, H4K16ac, and DAPI, respectively. Similar patterns were observed in all ten cells analyzed.

between FOXP3 and MOF throughout the nuclei in both MCF7 (Figures 3B and 3C) and 293T cells (data not shown). In order to confirm that the interaction between FOXP3 and MOF occurs on the chromatin, we performed immunofluorescent staining after in situ fractionation of the transfected cells. The procedure removed most of the cytoplasm, nuclear envelope, and nucleoplasm, as judged by disappearance of γ-tubulin and Lamin B1, while retained chromatin based on the H3 staining (Figure S6). As shown in Figure 3D, both MOF and H4K16ac overlapped with FOXP3, which confirmed the FOXP3-MOF interaction on the chromatin. We performed coimmunoprecipitation (coIP) to determine if MOF and overexpressed FOXP3 associate with each other. As shown in Figure 3E, an anti-MOF antibody targeting endogenous MOF brought down FOXP3 induced in the FOXP3-tet-off MCF7 cells. Furthermore, reciprocal coIP, using 293T cells where FOXP3 and MOF were exogenously expressed, unequivocally demonstrated that Myc-tagged FOXP3 and FLAG-tagged MOF physically interacted with each other (Figure 3F).

We took two approaches to rule out the possibility that their interaction was due to their association with DNA. First, we tested if the interaction can be disrupted by either ethidium bromide or pretreatment with DNase I. As shown in Figure 3G, neither treatment affected MOF-FOXP3 complex. Second, we evaluated if deletion of the forkhead DNA-binding domain prevented the FOXP3-MOF interaction. As shown in Figure 3H, the deletion mutant coprecipitated with the MOF.

Since the above studies involve FOXP3-transfected cells, we sought to confirm that the endogenous FOXP3 interact with endogenous MOF by both confocal microscopy and coIP. As shown in Figure 3I, essentially all FOXP3 (green dots) colocalized with MOF (red dots) in U2OS sarcoma cells. Perhaps because of an excess of MOF, not all MOF was found to be associated with endogenous FOXP3 in tumor cells. Given the important function of FOXP3 in Treg, we used coIP to determine if endogenous FOXP3 interact with MOF in Treg. As shown in Figure 3J, anti-MOF precipitated FOXP3. We have not been able to use anti-FOXP3 mAb to coprecipitate MOF. However, it is notable that even in the overexpression system, anti-FOXP3 mAb failed to coprecipitate MOF (data not shown). We suspect that the mAb we used blocked the FOXP3-MOF interaction, as the anti-Myc mAb precipitated both Myc-tagged FOXP3 and FLAG-tagged MOF from the same lysates (Figures 3F and 3H).

A Major Role of MOF in FOXP3-Mediated Global Gene Expression and Tumor Suppressive Function

In order to investigate whether MOF is required for FOXP3-dependent gene activation, we treated FOXP3-tet-off MCF7 cells with RNAi duplexes targeting endogenous MOF or control RNAi duplex (Figure 4A). In this model, induced FOXP3 expression was identical between control RNAi and MOF-RNAi-treated cells both in protein and mRNA levels (Figures 4A and 4C). Global mRNA expression analysis revealed that endogenous MOF knockdown impaired FOXP3-dependent gene activation in most, if not all, of the direct target genes (Figure 4B). Approximately 41.0% of target genes showed more than 30% impairment of FOXP3-mediated gene activation by MOF-RNAi as compared to control RNAi. In contrast, in FOXP3-mediated gene repression, the affected gene numbers and magnitude of impairments by the MOF knockdown seemed to be considerably smaller (Figure 4C). Thus, at the global level, MOF plays a more important role in FOXP3-mediated gene activation than in gene repression. Using real-time PCR, we confirmed the impacts of MOF knockdown on the FOXP3-dependent transcriptional activations of six randomly chosen activated target genes (Figure 4D).

Next, we sought to investigate whether MOF is also important for FOXP3-mediated biological consequences in epithelial cells, as well as for FOXP3-mediated gene regulation. Since FOXP3 in cancer cells showed significant cell growth suppression (Liu et al., 2009; Wang et al., 2009a; Zuo et al., 2007b), we tested if MOF knockdown would attenuate the growth suppressive function of FOXP3 in cancer cells. Interestingly, in this assay, only MOF knockdown without FOXP3 induction showed significant suppression of cell growth in MCF7 cells (Figure 4E), which is consistent with a recent report showing that *Mof* knockout significantly suppressed cell growth in mouse cells (Li et al., 2010). Despite such a progrowth function of MOF, the growth suppression by induced FOXP3 was significantly impaired by the MOF knockdown (Figures 4E and 4F), showing an important role of MOF in the tumor suppressive function of FOXP3.

Somatic Mutations of FOXP3 Disrupt FOXP3-MOF Colocalization in the Nuclei and Attenuate Acetylation of H4K16

In order to further investigate how FOXP3 and MOF interact with each other, we generated deletion and point mutants of FOXP3

(E) CoIP targeting endogenous MOF and induced FOXP3 in the FOXP3-tet-off MCF7 cells. A coIP was performed using an anti-MOF antibody. Precipitates were immunoblotted by an anti-FOXP3 antibody. Molecular weights are indicated to the left.

(F) Upper panel: FOXP3-myc/His and FLAG-MOF were expressed in 293T cells, coIP with an anti-myc antibody was performed, and the precipitants were immunoblotted by an anti-FLAG antibody. IgG-H: heavy chains of IgG. Molecular weight is indicated at the left side. Lower panels: Reciprocal coIP with the anti-FLAG antibody was performed. Since the FOXP3-myc/His overlapped with IgG-H signals in a 10% SDS-PAGE gel, we used 6% SDS-PAGE gels in this experiment, with a longer duration of electrophoresis. Immunoblots without primary myc-antibody were used to indicate the molecular sizes of IgG-H chains (lower panel).

(G) Reciprocal coIP was performed as in Figure 3F with ethidium bromide (EtBr) or with DNase I treatment. EtBr: IP reactions were performed in an IP buffer containing EtBr (100 μg/ml). DNase I: Before subjected to IP reaction, cell lysate was incubated with DNase I (10 U/ml) for 30 min at room temperature.

(H) FOXP3 lacking a forkhead domain (ΔC-FOXP3) and MOF were expressed in 293T cells, and reciprocal coIP was performed as in Figure 3F. A diagram of ΔC-FOXP3 is shown in the upper panel.

(I) A representative confocal image of U2OS sarcoma cells. Endogenous FOXP3 (green) and endogenous MOF (red) were stained by anti-FOXP3 and anti-MOF antibodies, respectively. White bars indicate 10 μm. Similar patterns were observed in at least five cells analyzed.

(J) Endogenous interaction between Foxp3 and Mof in CD25-positive mouse T cell population as revealed by coIP using anti-Foxp3 and anti-Mof antibodies.

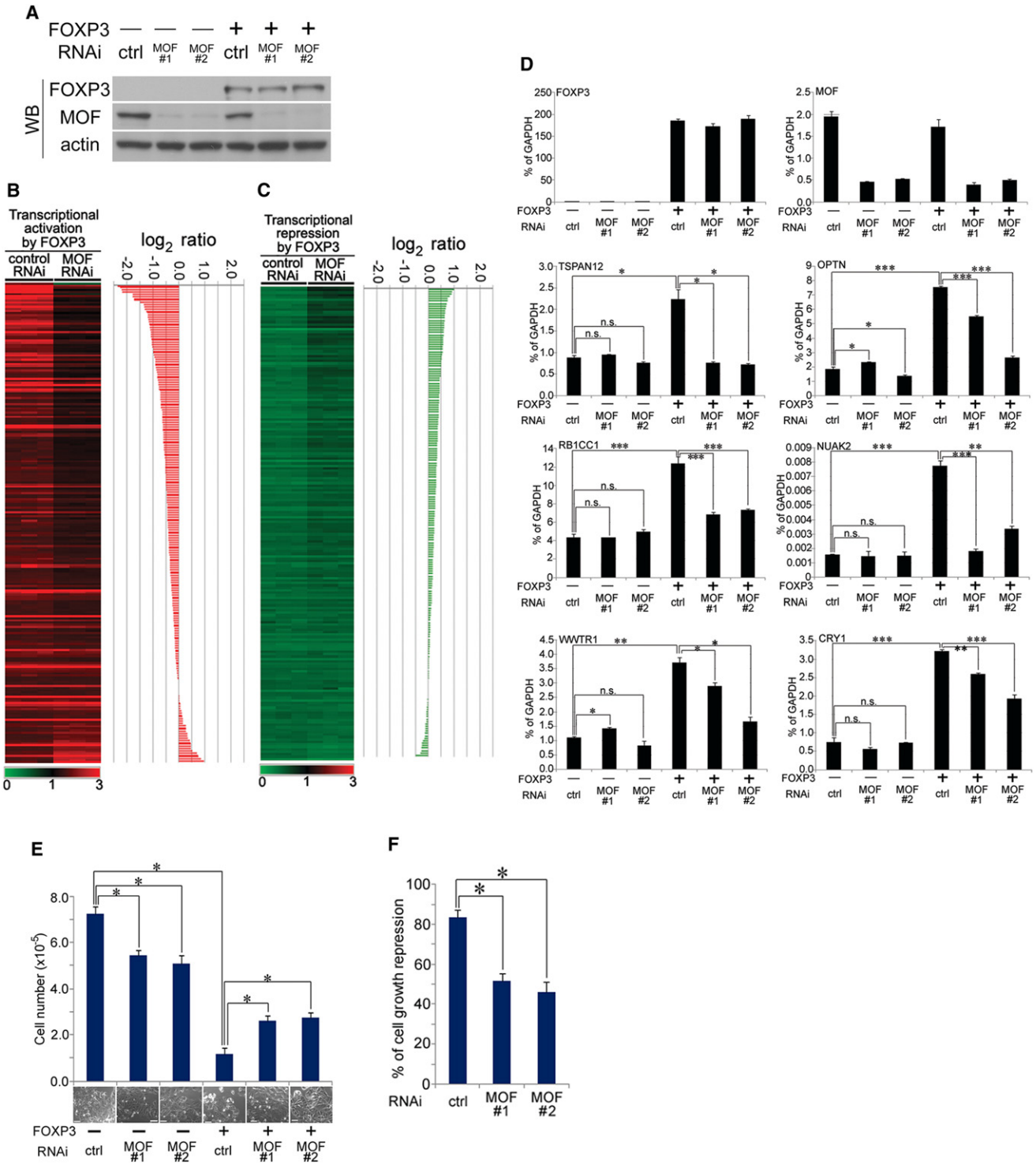

Figure 4. MOF Plays an Important Role in the FOXP3-Mediated Gene Activation and in the FOXP3-Dependent Cell Growth Repression

(A) RNAi-mediated knockdown of endogenous MOF was performed in the FOXP3-tet-off MCF7 cells together with FOXP3 induction. Protein expression levels of MOF and FOXP3 were examined by western blots with anti-MOF and anti-FOXP3 antibodies.

(B and C) Global mRNA expression analysis of direct target genes of FOXP3 with and without MOF knockdown. RNAi #2 was used in this analysis, as the knockdown is more efficient. (B) The heat map represents ratios of mRNA expressions before and after FOXP3 induction in control-RNAi and MOF-RNAi-treated MCF7 cells (expression values in cells without FOXP3 induction were normalized to 1.0). Color scale of the heat map is indicated at the bottom of the figure. (C) Bar graph represents log-scaled ratio of the relative mRNA expression between control-RNAi and MOF-RNAi groups. Dashed lines (red and green) represent log

(Figure 5A). MCF7 cells cotransfected with FLAG-MOF and FOXP3-myc/His mutants were examined by confocal microscopy. As shown in Figure 5B, full-length (FL) FOXP3 and N-terminal-deleted (ΔN) FOXP3 colocalized with MOF and, correspondingly, with H4K16ac in nucleus. Therefore, the N-terminal portion of FOXP3 does not regulate MOF-FOXP3 colocalization. Despite the subtle differences in the relative amounts of cytoplasmic-nuclear FOXP3, deletion mutants of either zinc finger (ZF) or leucine zipper (LZ) domains of FOXP3 (ΔZF or ΔLZ) accumulated in both cytoplasm and nuclei. In addition, these deletions had two significant effects. First, translocation of MOF to the central nuclear region was significantly reduced, with significant amounts of MOF protein accumulating in the peripheral nuclear region and the cytoplasm. Second, although substantial portions of ΔZF-FOXP3 and ΔLZ-FOXP3 did reach the central nuclear regions, much did not colocalize with MOF or H4K16ac. As expected, deletion of the C-terminal portion (ΔC) resulted in predominant cytoplasmic accumulation of FOXP3. Nevertheless, the cytoplasmic portion did not associate with MOF.

Since the ZF and LZ domains of FOXP3 are hot spots of somatic mutation in breast and prostate cancers (Wang et al., 2009a; Zuo et al., 2007b), we tested whether the somatic mutations in ZF or LZ domains affect the MOF-FOXP3 association. As shown in Figure 5C, mutations in the ZF domain, P202 > L (breast cancer) and G203 > R (prostate cancer), exhibited similar phenotypes to the ΔZF-FOXP3. Likewise, a mutation in the LZ domain, V239 > I (breast cancer), partially phenocopied the ΔLZ-FOXP3.

To further confirm the confocal microscope analysis, we performed an anti-H4K16ac-ChIP-qPCR. As shown in Figure 5D, in cells expressing ΔZF- or ΔLZ-FOXP3s, induction of H4K16ac at FOXP3-associated chromatin were significantly reduced as compared to those in cells expressing FL-FOXP3. Correspondingly, these FOXP3 mutants were largely inactive in both growth inhibition (Figure 5E) and induction of *p21* (Figure 5F). Importantly, GST pull-down assay revealed that GST-LZ but not GST-ZF interacted with MOF in vitro (Figure 5G), indicating a potential direct binding between MOF and the LZ domain of FOXP3. The interaction between FOXP3 and MOF was abrogated by the V239I mutation identified in human breast cancer tissue and blocked by synthetic peptide corresponding to amino acids 232–246 (CLLQREMVQSLEQQL) of FOXP3 (Figure 5H).

In order to investigate whether FOXP3 is important for the nuclear localization of MOF in vivo, we performed immunohistochemical staining of Mof using *Foxp*$^{-/y}$ or *Foxp3*$^{+/y}$ prostates from the *Foxp3*$^{fl/y}$PB-Cre^{+} and *Foxp3*$^{+/y}$ PB-Cre^{+} mice (Wang et al., 2009a). As shown in Figure 5I, in the prostate epithelial cells, significant amounts of Mof were detected in cytoplasm of the *Foxp3*$^{fl/y}$;PB-Cre^{+} cells, while the majority of Mof was accumulated in the nucleus in WT counterparts. Taken together, our data presented in this section demonstrated that FOXP3 directly interacts with MOF and regulates nuclear localization of MOF in both normal and cancer cells.

Both H4K16ac and H3K4me3 Are Required for FOXP3-Mediated Gene Activation

Since H4K16ac levels were significantly increased at FOXP3 binding sites regardless of whether the genes were activated or repressed, additional modifications should be required to determine the fate of FOXP3 targets. Apart from H4K16ac, H3K4me3 is an important mark of actively transcribed loci (Martin and Zhang, 2005). Moreover, it is known that MOF and MLL1 work in concert to simultaneously modify H4K16ac and H3K4me3 at promoters (Dou et al., 2005). Therefore we tested whether H3K4me3 correlated with FOXP3-dependent gene activation in MCF7 cells by an anti-H3K4me3-ChIP-qPCR. As shown in Figure 6A, FOXP3 increased H3K4me3 levels at activated binding sites, while no such impacts were observed at repressed binding sites. Consistent with the ChIP-qPCR, a confocal image showed that FOXP3 only partially overlapped with H3K4me3 (Figure 6B).

MOF (H4K16ac) and MLL1 complex (H3K4me3) work in concert to activate transcription (Dou et al., 2005). Therefore, we tested whether FOXP3 also recruits the MLL1 complex (i.e., MLL1, RbBP5, and WDR5) to its activated binding sites. As shown in Figure 6C, ChIP-qPCR indicated that the MLL1-complex proteins were detected at FOXP3-associated chromatin regardless of the FOXP3 induction. In order to explain how FOXP3 induces H3K4me3 at its activating binding sites, we carried out a motif scanning of the FOXP3-bound regions and searched for any enriched DNA motifs among activating and repressing binding sites. Apart from the FOXP3-binding motif (forkhead motif), the most enriched motif in the activated binding sites was a PLU-1-binding motif (Figure 7A). Interestingly, PLU-1 is a H3K4me3 demethylase and a putative oncogene for breast cancer (Yamane et al., 2007). Importantly, the enrichment of the PLU-1 motif was specific in FOXP3's activating binding sites (Figure 7A).

PLU-1 has a known DNA-binding motif (Figure 7B) (Scibetta et al., 2007). Strikingly, DNA-binding motifs of FOXP3 and PLU-1 were enriched at essentially overlapping regions (Figure 7C). This close proximity suggested a model in which FOXP3 binding may competitively displace PLU-1 from FOXP3-associated chromatin. To test this model, we evaluated whether FOXP3 binding reduced enrichments of PLU-1 at

(ratio) = +0.5 (ratio = 1.41) and = −0.5 (ratio = 0.71). The "direct target genes" were defined as (1) direct binding of FOXP3 between −2 kbp and +2 kbp from TSS of genes was revealed by ChIP-seq, and (2) mRNA expression values were increased to more than 1.5 times or decreased to less than 2/3 after FOXP3 induction in the control-RNAi-treated MCF7 cells. Ctrl: control.

(D) qRT-PCR was performed to examine mRNA levels of FOXP3's target genes with and without MOF knockdown.

(E and F) MOF contributes to FOXP3-mediated growth inhibition of cancer cells. (E) We plated 1.0 × 10^5 FOXP3-tet-off MCF7 cells into 6-well plates and treated them with either control- or MOF-RNAi. After 6 days of FOXP3 induction, cell numbers were counted. Microscopic pictures of the cells on day 6 are shown in the lower panel. White bars represent 20 μm. (F) Cell-growth repression rates—comparisons of cell numbers between FOXP3(-) and FOXP3(+) cells—in control- RNAi and MOF-RNAi-treated groups were calculated from the data in Figure 4E. Error bars in (E) and (F) represent +1 SD. p values were calculated by t test. *: $p < 0.05$; **: $p < 0.005$; ***: $p < 0.0005$. n.s.: not significant.

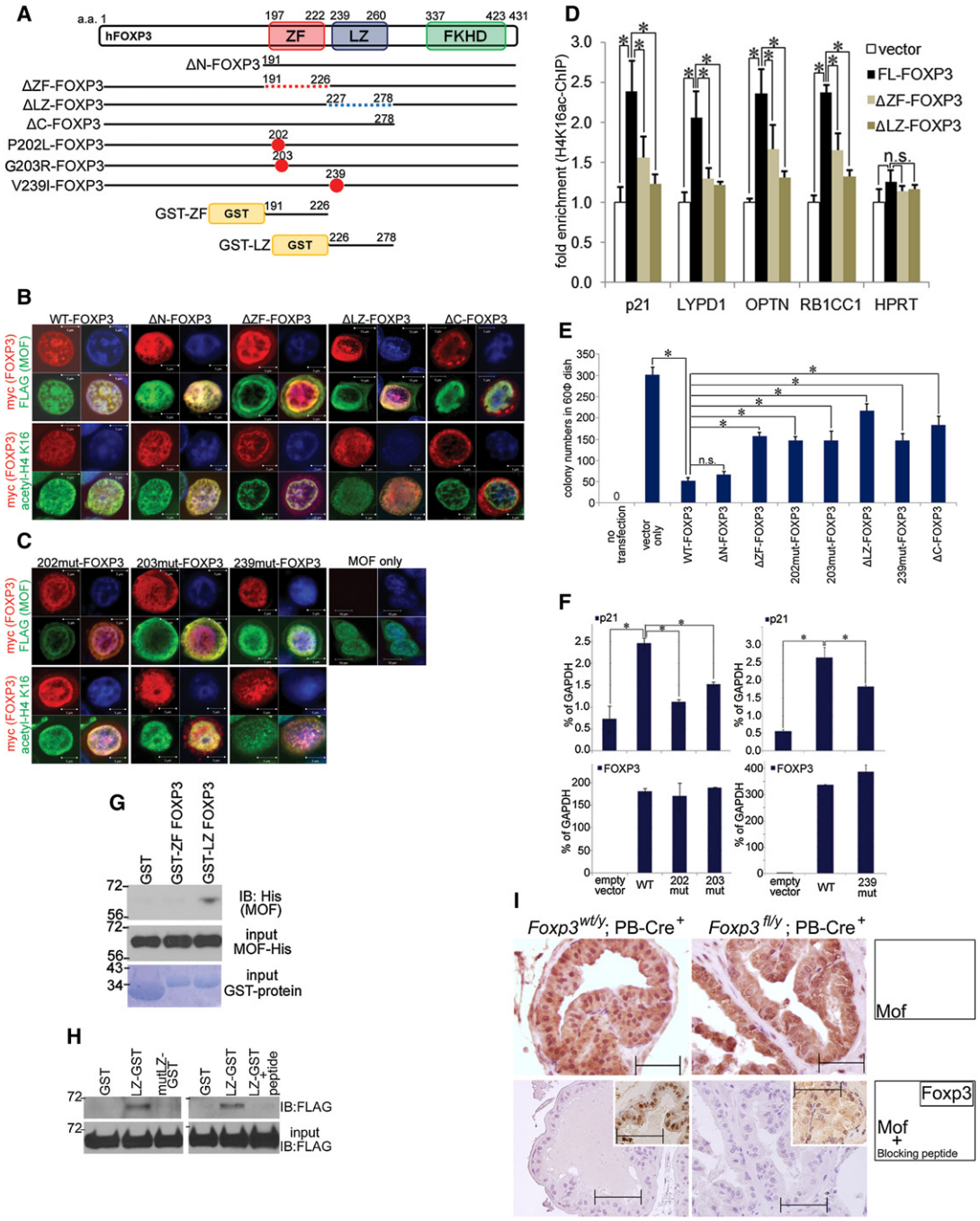

Figure 5. FOXP3 Mutations Abrogate the Proper Formation and Function of the FOXP3/MOF Complex

(A) A schematic view of the FOXP3 mutants used in this study. ZF, LZ, and FKHD represent zinc finger, leucine zipper, and forkhead domains, respectively. aa: amino acid positions. The red and blue dashed lines represent deleted regions in ΔZF- and ΔLZ-FOXP3, respectively. P202L and V239I were found in human breast cancers, and G203R was found in human prostate cancer. GST-fusion proteins used in this study are also indicated at the bottom.

(B and C) Representative confocal images. Deletion (B) and somatic mutation (C) series of FOXP3-myc/His together with FLAG-MOF were expressed in MCF7 cells, and cells were stained using anti-myc, anti-FLAG and anti-acetyl-H4K16 antibodies, as indicated. MCF7 cells transfected only with FLAG-MOF are also shown. White bars represent scale of objects. Similar patterns were observed in all five cells analyzed.

(D–F) (D) Full-length (FL) or deletion mutant FOXP3s were transfected into MCF7 cells. After 1 week of drug selection, ChIP-qPCR was performed using an anti-acetyl-H4K16 antibody. Enrichments of H4K16ac in the vector control cell were normalized to 1.0. (E) MCF7 cells were transfected with either vector, full-length FOXP3 or deletion/mutant-FOXP3, as indicated. After 2 weeks of blasticidin selection, cells were visualized by crystal violet dye, and colony numbers were counted. (F) MCF7 cells were transfected with either vector, WT-FOXP3 or mutant-FOXP3, as indicated. After 1 week of drug selection, RT-PCRs were performed. The y axis represents percentage of *GAPDH* expression. Error bars in (D)–(F) represent +1 SD. p values were calculated by t test. *: $p < 0.05$.

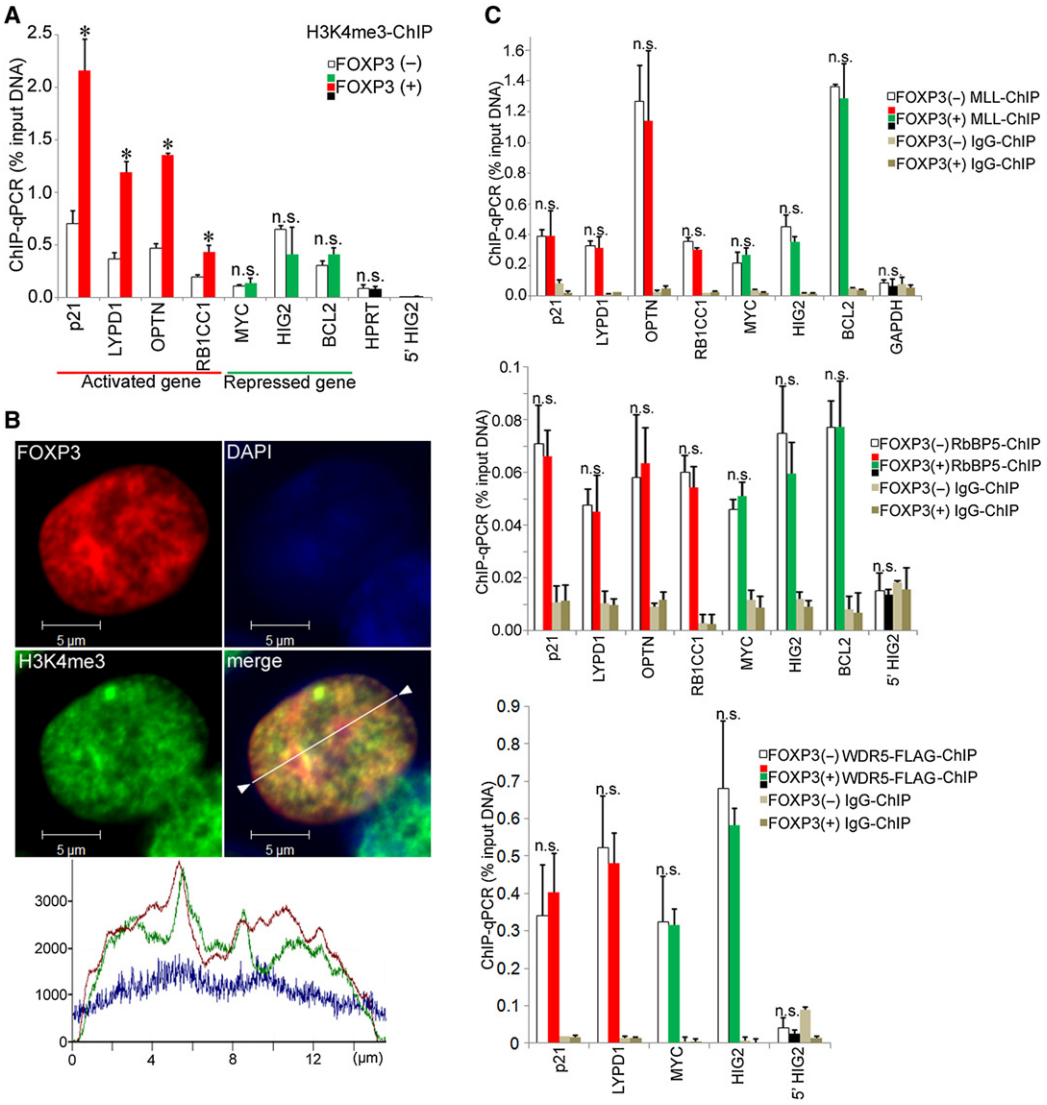

Figure 6. H3K4me3 Is Also Associated with the FOXP3-Mediated Gene Activation

(A) H3K4me3 levels at FOXP3-binding sites were examined by ChIP-qPCR before and after FOXP3 induction in the MCF7 cell. Error bars represent +1 SD of triplicate qPCR. *: $p < 0.05$ (t test). n.s.: not significant.

(B) A representative confocal image of FOXP3 (red) and H3K4me3 (green) in the MCF7 cell transfected with FOXP3. White bars represent 5 μm. Signal intensity profile of the confocal image is shown in the bottom panel. Red, green, and blue graphs indicate signal intensities of FOXP3, H3K4me3, and DAPI, respectively. A similar pattern was observed in 10/10 cells analyzed.

(C) ChIP-qPCRs targeting endogenous MLL1, endogenous RbBP5, and exogenously expressed FLAG-WDR5 were performed using anti-MLL1, anti-RbBP5, and anti-FLAG antibodies, respectively. White and colored (red, green, and black) bars represent percentage of input DNA before and after FOXP3 induction, respectively. GAPDH or 5′HIG2 were used as negative controls. Error bars represent +1 SD of triplicate qPCR. n.s.: not significant ($p > 0.05$, t test).

FOXP3-binding sites. Fifteen activated and 11 repressed genes were chosen according to the following criteria: (1) genes whose expression was strongly affected by FOXP3—more than twice or less than half, compared to FOXP3(-) cells, and (2) both of the FOXP3 and PLU-1 motifs were identified around ChIP-seq peaks (within 500 bp of the ChIP-seq peaks). As shown in Figure 7D,

(G) GST pull-down assay was performed using GST-FOXP3 domains and His-MOF proteins as indicated.

(H) Left panel: Beads conjugated with either GST, LZ-GST, or mutLZ(V239I)-GST were incubated with FLAG-MOF transfected 293T cell lysate. Precipitates were subjected to an immunoblot using anti-FLAG antibody. Right panel: GST pull-down assay using LZ-GST-conjugated beads was performed, incubating with and without a blocking peptide corresponding to amino acids 232–246 of FOXP3 (CLLQREMVQSLEQQL).

(I) Immunohistochemical staining using an anti-Mof antibody was performed using mouse prostate tissues, with and without prostate-specific knockout of *Foxp3* (16-week-old *Foxp3*$^{fl/y}$;PB-Cre^{+} and *Foxp3*$^{wt/y}$;PB-Cre^{+} mice, respectively). Mof staining with a blocking peptide is shown as a negative control. Foxp3 staining is shown in the inserts. Black bars represent 50 μm.

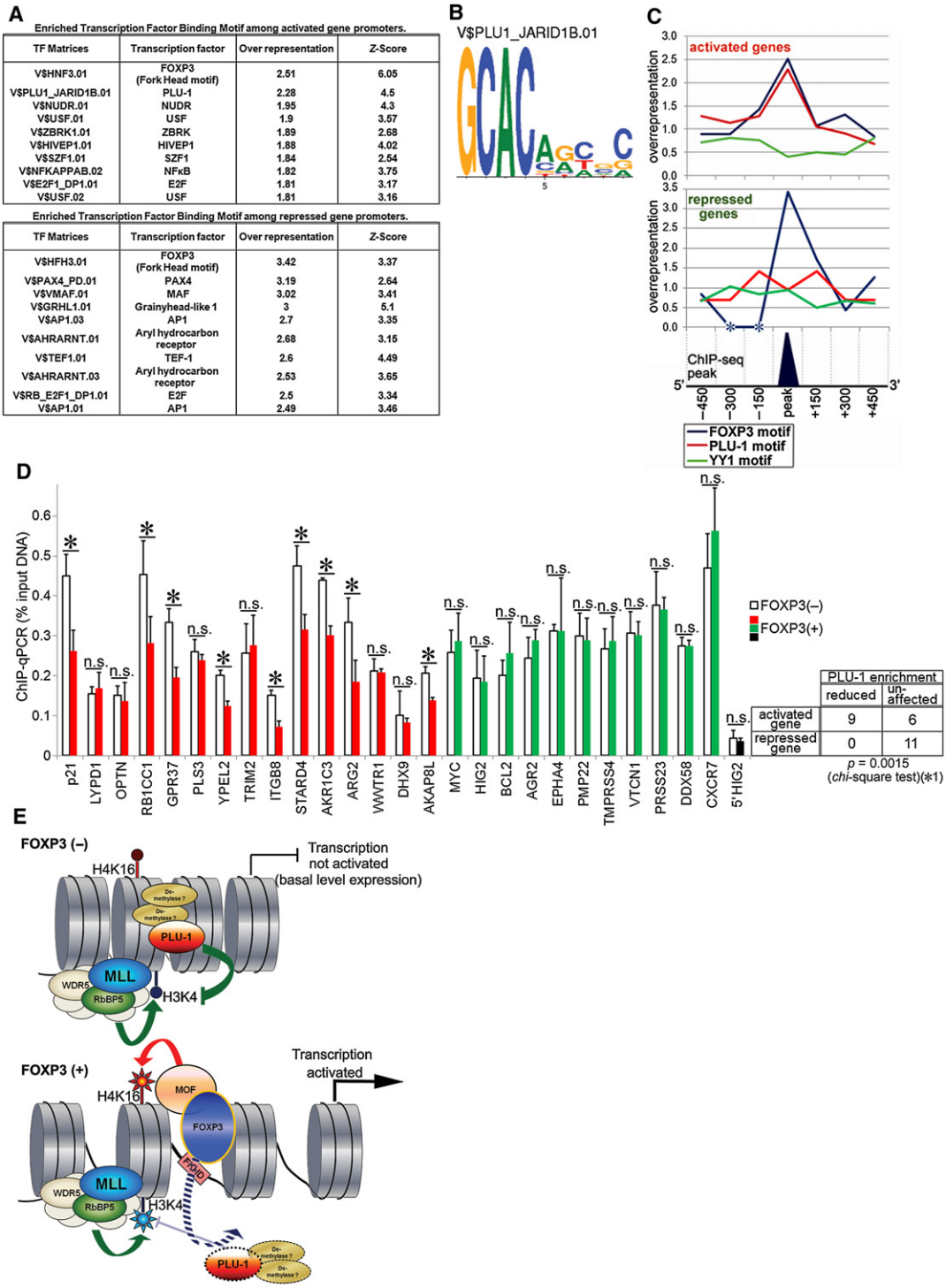

Figure 7. FOXP3 Facilitates H3K4me3 Presumably by Replacing Histone Demethylase(s) from Its Binding Sites: A Hypothetical Model

(A) Transcription-factor-binding motifs that were significantly enriched among FOXP3-binding sites at either activated or repressed gene promoters are listed. Top ten ranked motifs as sorted by overrepresentation scores were included. Statistical significances were evaluated by Z score according to the database http://www.genomatix.de.

(B) A known DNA-binding motif of PLU-1.

(C) Genomic regions around the FOXP3-ChIP-seq peaks were partitioned into 150 bp windows, and enrichments of the forkhead (FOXP3) and PLU-1 motifs among each of these 150 bp partitions are evaluated by the overrepresentation scores as in Figure 7A. The YY1 motif was used as an unrelated negative control. *: forkhead motifs were not identified in these regions.

induction of FOXP3 significantly reduced the binding of PLU-1 at 9 out of 15 activated promoters. FOXP3 and PLU-1 motifs were essentially overlapped at *p21*, *YPEL2*, and *ITGB8* promoters and located closely at other promoters (Figure S7). Interestingly, the distance between FOXP3 and PLU-1 motifs is likely a major contributor to the displacements of PLU-1 caused by FOXP3, as all nine genes that showed significant displacements of PLU-1 had FOXP3 motifs within 100 bp from the PLU-1 motif (Figure S8). However, proximity of the binding sites is not sufficient, since displacements were not observed in two genes with a distance of <100 bp (Figure S8). Importantly, no displacements of PLU-1 were observed among repressed genes (Figure 7D). Since JARID1 family members may not always bind to chromatin in a DNA sequence-specific fashion, it is possible that, at the repressed promoters, PLU-1 binds to other chromatin-associated proteins and is not displaced when FOXP3 binds to the loci.

DISCUSSION

Our integrated analysis of FOXP3-binding sites and gene regulation presented herein identified 845 direct targets in a cancer cell. The most remarkable feature of the FOXP3-binding sites is their proximity to TSS. Such proximity strongly suggests a direct involvement of FOXP3 in the regulation of transcription. The precise identification of FOXP3-binding sites also allows us to define how FOXP3 coordinates local histone modifications (Jenuwein and Allis, 2001; Lee et al., 2010). We have demonstrated a broad requirement of MOF in FOXP3-mediated gene activation, while the impact of MOF knockdown on FOXP3-dependent gene repression was negligible. Surprisingly, FOXP3 induces local H4K16ac regardless of whether the genes are activated or repressed. The strong association between FOXP3 and H4K16ac is due to a direct interaction between FOXP3 and MOF. These data raise two intriguing issues. First, how can the H4K16ac be recognized as a part of repressive histone codes in FOXP3-mediated gene repression? While a definitive answer remains to be elucidated, it is of note that in embryonic stem cells, H3K4me3 and H3K27me3 can frequently be observed at the same loci in transcriptionally silenced genes (Mikkelsen et al., 2007; Pan et al., 2007; Vastenhouw et al., 2010). The authors proposed a bivalent histone code in which a mixture of activating (H3K4me3) and repressive (H3K27me3) histone codes could be read as a repressive code. Since repressed targets of FOXP3 exhibit significantly increased H3K27me3 levels, it is likely that H3K27me3 (repressive code) somehow overrides the H4K16ac (activating code) to cause gene silencing at FOXP3-associated chromatin. Second, what other histone modifications cooperate with H4K16ac to constitute activating histone codes for the activated target genes? Considering a previous report demonstrating that MLL1 complex cooperates with MOF in Hox gene activation (Dou et al., 2005), we tested whether FOXP3 also recruits MLL1 complex to activate target genes. In this case, although MLL1 complexes were found at FOXP3 target sites, their recruitments are FOXP3-independent. Of note, since FOXP3 recruited neither RbBP5 nor WDR5 to its binding sites, it is unlikely that other MLL/SET1 family methyltransferases are recruited by FOXP3. Steady state levels of H3K4me3 can be maintained by both H3K4 methyltransferases and H3K4 demethylases (Shi et al., 2004; Shi and Whetstine, 2007; Yamane et al., 2007). Since our ChIP-qPCR revealed that FOXP3-binding sites are basically decorated with MLL1 even before FOXP3 inductions, it is intriguing that displacements of H3K4 demethylase(s) may explain how the H3K4me3 is induced by FOXP3. We identified closely located enrichments of FOXP3 and PLU-1 motifs specifically among activated targets. This selectivity prompted us to test and confirm a hypothesis that FOXP3 causes displacement of PLU-1 from at least a major subset of activated FOXP3-binding regions. We demonstrated that FOXP3 significantly displaced PLU-1 at 9 out of 15 (60.0%) activated targets tested. It would be of interest to determine whether displacement of other H3K4me3 demethylases is responsible for activation of FOXP3 targets.

H3K4me3 recruits various downstream effectors to activate transcription of the loci (Chi et al., 2010; Levy and Gozani, 2010; Ruthenburg et al., 2007). For example, chromatin remodeling NURF complex and PHD finger-containing ING family and human SAGA complexes can specifically recognize H3K4me3 (Chi et al., 2010; Levy and Gozani, 2010; Vermeulen et al., 2010). Among them, BPTF in NURF complex is of particular interest, since BPTF can recognize both H3K4me3 and H4K16ac by its PHD and bromo domains, respectively (Kwon et al., 2009; Wysocka et al., 2006). A more recent study demonstrated that the H3K4me3 and H4K16ac combination is selectively recognized by BPTF if they are present in the same mononucleosome (Ruthenburg et al., 2011). It is plausible that BPTF may be selectively recruited to the FOXP3-bound chromatins to initiate chromatin remodeling necessary for transcriptional activation.

Based on these considerations, we hereby propose a model by which FOXP3 activates multiple, although not necessarily all, target genes (Figure 7E). In essence, FOXP3 pulls MOF to its binding sites, where the MOF induces H4K16ac. Perhaps by competitive DNA binding or other unknown mechanisms, FOXP3 causes displacement of H3K4 demethylase(s) from FOXP3-binding sites and thereby increases H3K4me3. FOXP3 may thus create a histone code (H4K16ac/H3K4me3) locally, perhaps within a nucleosome, which leads to active transcription, as recently reported by Ruthenburg et al. (2011).

Our data provided here also explain a mechanism for functional inactivation of FOXP3 protein in cancer cells. We presented direct evidence that MOF is required not only for FOXP3-mediated gene activation but also for FOXP3-dependent cell-growth suppression in cancer cells. Therefore, it is not surprising that this interaction is targeted during tumorigenesis,

(D) ChIP-qPCR was performed using an anti-PLU-1 antibody targeting endogenous PLU-1 before and after FOXP3 induction. The y axis represents qPCR signals (percentage of input DNA). Error bars represent +1 SD of triplicate qPCR. *: $p < 0.05$ (t test). n.s.: not significant. (*1) p value was calculated by chi-square test. With Yates modification: $p = 0.0058$. Fisher's exact test: $p = 0.0024$.
(E) A proposed model by which FOXP3 activates multiple gene expression by pulling MOF and causing displacement of H3K4me demethylase(s).

as demonstrated herein. Our data is consistent with previous reports that MOF expression is frequently downregulated in tumors (Pfister et al., 2008) and that global H4K16ac levels are significantly reduced in breast cancer cells (Fraga et al., 2005). Paradoxically, it was recently reported that MOF promotes the survival of mouse embryonic fibroblasts (Li et al., 2010). Likewise, our data also showed that, in the absence of FOXP3, silencing of *MOF* retarded the growth of MCF7 cells. Therefore, the function of MOF in growth likely depends on the activity of other tumor suppressors. Since our data showed that aberrant expression of FOXP3 affects nuclear localization of MOF, it is of interest to determine whether the documented defects of FOXP3 nuclear localization (Katoh et al., 2010; Ladoire et al., 2011; Wang et al., 2010) explain defective H4K16ac in clinical breast cancer samples (Fraga et al., 2005).

EXPERIMENTAL PROCEDURES

Cell Lines, Plasmids, Bacterial Expression Vectors, and Oligonucleotides

An MCF7 human breast cancer cell line with a FOXP3-tet-off system was described previously (Zuo et al., 2007b). 293T and MCF7 cells were cultured with DMEM supplemented with 10% FBS and P/S. FOXP3-myc/His, 3×FLAG -MOF and -WDR5 were cloned into pcDNA6 (Invitrogen, CA) and p3×FLAG-CMV-7.1 (Sigma Aldrich, MO) vectors, respectively. Deletion constructs of FOXP3 and mutant FOXP3s were cloned using GeneTailor Site-Directed Mutagenesis System (Invitrogen), using pcDNA6-FOXP3-myc/His as a template according to the manufacturer's protocol. Leucine zipper and zinc finger domains of FOXP3 were cloned into pGEX-KG vector (ATCC, VA). DNA and RNAi oligonucleotides used in this study are listed in Table S4.

Antibodies

Commercial antibodies used in this study were as follows: mouse anti-FOXP3 (eBio7979, eBioscience, CA), rabbit anti-MOF (A300–992A, Bethyl Laboratories, TX), mouse anti-actin (ab3280, ABcam, MA), rabbit anti-acetyl-H4 at K16 (#07-329, Millipore, MA), rabbit anti-trimethyl-H3 at K4 (#9727, Cell Signaling, MA), rabbit anti-acetyl-H3 (#9677, Cell Signaling), rabbit anti-trimethyl-H3 at K27 (#07-449, Millipore), rabbit anti-RbBP5 (A300–109A, Bethyl Laboratories), rabbit anti-PLU-1 (ab50958, ABcam), mouse anti-FLAG (clone M2, Sigma Aldrich), mouse anti-myc (9E10, Covance, NJ), mouse anti-6×His (34660, QIAGEN, MA), goat anti-mouse IgG Alexa Fluor 568-conjugated (A11031, Invitrogen), and goat anti-rabbit IgG Alexa Fluor 488-conjugated (A11034, Invitrogen). For immunofluorescent staining of U2OS cells, rabbit anti-FOXP3 (ab10563, ABcam) and mouse anti-PLU-1 (ab54276, ABcam) were used. Rabbit anti-MLL1c antibody was raised as described previously (Dou et al., 2005). Blocking peptide for the MOF antibody (BP300-992) was used for immunohistochemistry.

ChIP-Sequence and Data Analysis

ChIP DNA libraries were modified for sequencing using ChIP-Seq Sample Prep Kit (Illumina, CA) according to the manufacturer's protocol. ChIP-seq was performed using Illumina Genome Analyzer (Illumina) as described previously (Yu et al., 2010). Briefly, raw sequence image data were processed by Illumina analysis pipeline, aligned onto unmasked human genome (NCBI v36, hg18) using ELAND software (Illumina). Hpeak, a Hidden Markov Model (HMM)-based peak-identifying algorithm (Qin et al., 2010), was used. Assuming the average size of ChIP-DNA fragments was 200 bp (range: 175–225 bp), we extended each of the 36 bp sequencing read to make a 200 bp hypothetical genomic DNA fragment (HDF). Under the null hypothesis of no enrichment in the FOXP3-ChIP treated sample versus IgG-ChIP control sample, the numbers of HDFs from the two libraries were assumed to follow the same distribution. The entire genome was partitioned into 25 bp windows and HMM was applied to define where FOXP3-enriched regions start and end. Assignments of ChIP-seq peaks with coding genes were defined as follows: (1) if a binding site locates in introns or exons of a gene, it was assigned to this gene; (2) if a site is between genes, it was assigned to the nearest downstream gene. Searching for transcription factor binding motifs was performed using MatInspector (Cartharius et al., 2005), as part of the Genomatix software suite (Genomatix Software GmbH, Munich, Germany) (www.genomatix.de). Over-representations of motifs in the FOXP3 ChIP-enriched peaks were evaluated against length-matched control sequences that were randomly selected from human promoter genomic sequences.

Immunofluorescence after In Situ Subcellular Fractionation

FOXP3-myc/His and FLAG-MOF were transfected into MCF7 cells. Before proceeding to fixations for immunofluorescent stainings, in situ subcellular fractionation was performed as described (Sawasdichai et al., 2010) with some modifications. Briefly: (1) the cytoplasmic fraction of the cells was removed by incubating culture slides on ice for 1 min in a buffer containing 10 mM PIPES, 300 mM sucrose, 100 mM NaCl, 3mM MgCl2, 1mM EGTA, and 0.1% Triton-X; (2) the culture slides were washed twice by PBS; (3) the nuclear fraction of the cells was removed by incubating the culture slides on ice for 20 min in a buffer containing 10 mM PIPES, 300 mM sucrose, 100 mM NaCl, 3 mM MgCl2, 1 mM EGTA, and 0.5% Triton-X; (4) the culture slides were washed three times by PBS; (5) Immunofluorescent stainings were then performed.

SUPPLEMENTAL INFORMATION

Supplemental Information includes eight figures, four tables, and Supplemental References and can be found with this article online at doi:10.1016/j.molcel.2011.10.012.

ACKNOWLEDGMENTS

H.K. is a recipient of a Postdoctoral Fellowship Award from the Breast Cancer Research Program, Department of Defense. This work has been supported by grants from the National Institutes of Health and the U.S. Department of Defense and a grant from the Ministry of Sciences and Technology of China (2009DFB30310). We are grateful to Jindan Yu for critical reading of the manuscript and Chun-Shu Wong for editorial assistance.

Received: January 3, 2011
Revised: August 15, 2011
Accepted: October 10, 2011
Published: December 8, 2011

REFERENCES

Bennett, C.L., Christie, J., Ramsdell, F., Brunkow, M.E., Ferguson, P.J., Whitesell, L., Kelly, T.E., Saulsbury, F.T., Chance, P.F., and Ochs, H.D. (2001). The immune dysregulation, polyendocrinopathy, enteropathy, X-linked syndrome (IPEX) is caused by mutations of FOXP3. Nat. Genet. *27*, 20–21.

Birzele, F., Fauti, T., Stahl, H., Lenter, M.C., Simon, E., Knebel, D., Weith, A., Hildebrandt, T., and Mennerich, D. (2011). Next-generation insights into regulatory T cells: expression profiling and FoxP3 occupancy in Human. Nucleic Acids Research *39*, 7946–7960.

Brunkow, M.E., Jeffery, E.W., Hjerrild, K.A., Paeper, B., Clark, L.B., Yasayko, S.A., Wilkinson, J.E., Galas, D., Ziegler, S.F., and Ramsdell, F. (2001). Disruption of a new forkhead/winged-helix protein, scurfin, results in the fatal lymphoproliferative disorder of the scurfy mouse. Nat. Genet. *27*, 68–73.

Cartharius, K., Frech, K., Grote, K., Klocke, B., Haltmeier, M., Klingenhoff, A., Frisch, M., Bayerlein, M., and Werner, T. (2005). MatInspector and beyond: promoter analysis based on transcription factor binding sites. Bioinformatics *21*, 2933–2942.

Chatila, T.A., Blaeser, F., Ho, N., Lederman, H.M., Voulgaropoulos, C., Helms, C., and Bowcock, A.M. (2000). JM2, encoding a fork head-related protein, is mutated in X-linked autoimmunity-allergic disregulation syndrome. J. Clin. Invest. *106*, R75–R81.

Chi, P., Allis, C.D., and Wang, G.G. (2010). Covalent histone modifications—miswritten, misinterpreted and mis-erased in human cancers. Nat. Rev. Cancer *10*, 457–469.

Dalgliesh, G.L., Furge, K., Greenman, C., Chen, L., Bignell, G., Butler, A., Davies, H., Edkins, S., Hardy, C., Latimer, C., et al. (2010). Systematic sequencing of renal carcinoma reveals inactivation of histone modifying genes. Nature *463*, 360–363.

Dion, M.F., Altschuler, S.J., Wu, L.F., and Rando, O.J. (2005). Genomic characterization reveals a simple histone H4 acetylation code. Proc. Natl. Acad. Sci. USA *102*, 5501–5506.

Dou, Y., Milne, T.A., Tackett, A.J., Smith, E.R., Fukuda, A., Wysocka, J., Allis, C.D., Chait, B.T., Hess, J.L., and Roeder, R.G. (2005). Physical association and coordinate function of the H3 K4 methyltransferase MLL1 and the H4 K16 acetyltransferase MOF. Cell *121*, 873–885.

Duns, G., van den Berg, E., van Duivenbode, I., Osinga, J., Hollema, H., Hofstra, R.M., and Kok, K. (2010). Histone methyltransferase gene SETD2 is a novel tumor suppressor gene in clear cell renal cell carcinoma. Cancer Res. *70*, 4287–4291.

Fontenot, J.D., Gavin, M.A., and Rudensky, A.Y. (2003). Foxp3 programs the development and function of CD4+CD25+ regulatory T cells. Nat. Immunol. *4*, 330–336.

Fraga, M.F., Ballestar, E., Villar-Garea, A., Boix-Chornet, M., Espada, J., Schotta, G., Bonaldi, T., Haydon, C., Ropero, S., Petrie, K., et al. (2005). Loss of acetylation at Lys16 and trimethylation at Lys20 of histone H4 is a common hallmark of human cancer. Nat. Genet. *37*, 391–400.

Hori, S., Nomura, T., and Sakaguchi, S. (2003). Control of regulatory T cell development by the transcription factor Foxp3. Science *299*, 1057–1061.

Jenuwein, T., and Allis, C.D. (2001). Translating the histone code. Science *293*, 1074–1080.

Katoh, H., Zheng, P., and Liu, Y. (2010). Signalling through FOXP3 as an X-linked tumor suppressor. Int. J. Biochem. Cell Biol. *42*, 1784–1787.

Kleer, C.G., Cao, Q., Varambally, S., Shen, R., Ota, I., Tomlins, S.A., Ghosh, D., Sewalt, R.G., Otte, A.P., Hayes, D.F., et al. (2003). EZH2 is a marker of aggressive breast cancer and promotes neoplastic transformation of breast epithelial cells. Proc. Natl. Acad. Sci. USA *100*, 11606–11611.

Kwon, S.Y., Xiao, H., Wu, C., and Badenhorst, P. (2009). Alternative splicing of NURF301 generates distinct NURF chromatin remodeling complexes with altered modified histone binding specificities. PLoS Genet. *5*, e1000574.

Ladoire, S., Arnould, L., Mignot, G., Coudert, B., Rébé, C., Chalmin, F., Vincent, J., Bruchard, M., Chauffert, B., Martin, F., et al. (2011). Presence of Foxp3 expression in tumor cells predicts better survival in HER2-overexpressing breast cancer patients treated with neoadjuvant chemotherapy. Breast Cancer Res. Treat. *125*, 65–72.

Lee, K.K., and Workman, J.L. (2007). Histone acetyltransferase complexes: one size doesn't fit all. Nat. Rev. Mol. Cell Biol. *8*, 284–295.

Lee, J.S., Smith, E., and Shilatifard, A. (2010). The language of histone crosstalk. Cell *142*, 682–685.

Levy, D., and Gozani, O. (2010). Decoding chromatin goes high tech. Cell *142*, 844–846.

Li, X., and Dou, Y. (2010). New perspectives for the regulation of acetyltransferase MOF. Epigenetics *5*, 185–188.

Li, B., Samanta, A., Song, X., Iacono, K.T., Bembas, K., Tao, R., Basu, S., Riley, J.L., Hancock, W.W., Shen, Y., et al. (2007). FOXP3 interactions with histone acetyltransferase and class II histone deacetylases are required for repression. Proc. Natl. Acad. Sci. USA *104*, 4571–4576.

Li, X., Corsa, C.A., Pan, P.W., Wu, L., Ferguson, D., Yu, X., Min, J., and Dou, Y. (2010). MOF and H4 K16 acetylation play important roles in DNA damage repair by modulating recruitment of DNA damage repair protein Mdc1. Mol. Cell. Biol. *30*, 5335–5347.

Liu, R., Wang, L., Chen, G., Katoh, H., Chen, C., Liu, Y., and Zheng, P. (2009). FOXP3 up-regulates p21 expression by site-specific inhibition of histone deacetylase 2/histone deacetylase 4 association to the locus. Cancer Res. *69*, 2252–2259.

Liu, Y., Wang, L., and Zheng, P. (2010). X-linked tumor suppressors: perplexing inheritance, a unique therapeutic opportunity. Trends Genet. *26*, 260–265.

Lu, C., Han, H.D., Mangala, L.S., Ali-Fehmi, R., Newton, C.S., Ozbun, L., Armaiz-Pena, G.N., Hu, W., Stone, R.L., Munkarah, A., et al. (2010). Regulation of tumor angiogenesis by EZH2. Cancer Cell *18*, 185–197.

Marson, A., Kretschmer, K., Frampton, G.M., Jacobsen, E.S., Polansky, J.K., MacIsaac, K.D., Levine, S.S., Fraenkel, E., von Boehmer, H., and Young, R.A. (2007). Foxp3 occupancy and regulation of key target genes during T-cell stimulation. Nature *445*, 931–935.

Martin, C., and Zhang, Y. (2005). The diverse functions of histone lysine methylation. Nat. Rev. Mol. Cell Biol. *6*, 838–849.

Mikkelsen, T.S., Ku, M., Jaffe, D.B., Issac, B., Lieberman, E., Giannoukos, G., Alvarez, P., Brockman, W., Kim, T.K., Koche, R.P., et al. (2007). Genome-wide maps of chromatin state in pluripotent and lineage-committed cells. Nature *448*, 553–560.

Minucci, S., and Pelicci, P.G. (2006). Histone deacetylase inhibitors and the promise of epigenetic (and more) treatments for cancer. Nat. Rev. Cancer *6*, 38–51.

Mosammaparast, N., and Shi, Y. (2010). Reversal of histone methylation: biochemical and molecular mechanisms of histone demethylases. Annu. Rev. Biochem. *79*, 155–179.

Pan, G., Tian, S., Nie, J., Yang, C., Ruotti, V., Wei, H., Jonsdottir, G.A., Stewart, R., and Thomson, J.A. (2007). Whole-genome analysis of histone H3 lysine 4 and lysine 27 methylation in human embryonic stem cells. Cell Stem Cell *1*, 299–312.

Pan, F., Yu, H., Dang, E.V., Barbi, J., Pan, X., Grosso, J.F., Jinasena, D., Sharma, S.M., McCadden, E.M., Getnet, D., et al. (2009). Eos mediates Foxp3-dependent gene silencing in CD4+ regulatory T cells. Science *325*, 1142–1146.

Pfister, S., Rea, S., Taipale, M., Mendrzyk, F., Straub, B., Ittrich, C., Thuerigen, O., Sinn, H.P., Akhtar, A., and Lichter, P. (2008). The histone acetyltransferase hMOF is frequently downregulated in primary breast carcinoma and medulloblastoma and constitutes a biomarker for clinical outcome in medulloblastoma. Int. J. Cancer *122*, 1207–1213.

Qin, Z.S., Yu, J., Shen, J., Maher, C.A., Hu, M., Kalyana-Sundaram, S., Yu, J., and Chinnaiyan, A.M. (2010). HPeak: an HMM-based algorithm for defining read-enriched regions in ChIP-Seq data. BMC Bioinformatics *11*, 369.

Robinson, P.J., An, W., Routh, A., Martino, F., Chapman, L., Roeder, R.G., and Rhodes, D. (2008). 30 nm chromatin fibre decompaction requires both H4-K16 acetylation and linker histone eviction. J. Mol. Biol. *381*, 816–825.

Ruthenburg, A.J., Allis, C.D., and Wysocka, J. (2007). Methylation of lysine 4 on histone H3: intricacy of writing and reading a single epigenetic mark. Mol. Cell *25*, 15–30.

Ruthenburg, A.J., Li, H., Milne, T.A., Dewell, S., McGinty, R.K., Yuen, M., Ueberheide, B., Dou, Y., Muir, T.W., Patel, D.J., and Allis, C.D. (2011). Recognition of a mononucleosomal histone modification pattern by BPTF via multivalent interactions. Cell *145*, 692–706.

Sadlon, T.J., Wilkinson, B.G., Pederson, S., Brown, C.Y., Bresatz, S., Gargett, T., Melville, E.L., Peng, K., D'Andrea, R.J., Glonek, G.G., et al. (2010). Genome-wide identification of human FOXP3 target genes in natural regulatory T cells. J. Immunol. *185*, 1071–1081.

Sawasdichai, A., Chen, H.T., Abdul Hamid, N., Jayaraman, P.S., and Gaston, K. (2010). In situ subcellular fractionation of adherent and non-adherent mammalian cells. J. Vis. Exp. *41*, e1958. 10.3791/1958.

Scibetta, A.G., Santangelo, S., Coleman, J., Hall, D., Chaplin, T., Copier, J., Catchpole, S., Burchell, J., and Taylor-Papadimitriou, J. (2007). Functional analysis of the transcription repressor PLU-1/JARID1B. Mol. Cell. Biol. *27*, 7220–7235.

Shi, Y., and Whetstine, J.R. (2007). Dynamic regulation of histone lysine methylation by demethylases. Mol. Cell *25*, 1–14.

Shi, Y., Lan, F., Matson, C., Mulligan, P., Whetstine, J.R., Cole, P.A., Casero, R.A., and Shi, Y. (2004). Histone demethylation mediated by the nuclear amine oxidase homolog LSD1. Cell *119*, 941–953.

Shogren-Knaak, M., Ishii, H., Sun, J.M., Pazin, M.J., Davie, J.R., and Peterson, C.L. (2006). Histone H4-K16 acetylation controls chromatin structure and protein interactions. Science *311*, 844–847.

Smith, E.R., Cayrou, C., Huang, R., Lane, W.S., Côté, J., and Lucchesi, J.C. (2005). A human protein complex homologous to the Drosophila MSL complex is responsible for the majority of histone H4 acetylation at lysine 16. Mol. Cell. Biol. *25*, 9175–9188.

Strahl, B.D., and Allis, C.D. (2000). The language of covalent histone modifications. Nature *403*, 41–45.

Taipale, M., Rea, S., Richter, K., Vilar, A., Lichter, P., Imhof, A., and Akhtar, A. (2005). hMOF histone acetyltransferase is required for histone H4 lysine 16 acetylation in mammalian cells. Mol. Cell. Biol. *25*, 6798–6810.

Vastenhouw, N.L., Zhang, Y., Woods, I.G., Imam, F., Regev, A., Liu, X.S., Rinn, J., and Schier, A.F. (2010). Chromatin signature of embryonic pluripotency is established during genome activation. Nature *464*, 922–926.

Vermeulen, M., Eberl, H.C., Matarese, F., Marks, H., Denissov, S., Butter, F., Lee, K.K., Olsen, J.V., Hyman, A.A., Stunnenberg, H.G., and Mann, M. (2010). Quantitative interaction proteomics and genome-wide profiling of epigenetic histone marks and their readers. Cell *142*, 967–980.

Wang, L., Liu, R., Li, W., Chen, C., Katoh, H., Chen, G.Y., McNally, B., Lin, L., Zhou, P., Zuo, T., et al. (2009a). Somatic single hits inactivate the X-linked tumor suppressor FOXP3 in the prostate. Cancer Cell *16*, 336–346.

Wang, Z., Zang, C., Cui, K., Schones, D.E., Barski, A., Peng, W., and Zhao, K. (2009b). Genome-wide mapping of HATs and HDACs reveals distinct functions in active and inactive genes. Cell *138*, 1019–1031.

Wang, L., Liu, R., Ribick, M., Zheng, P., and Liu, Y. (2010). FOXP3 as an X-linked tumor suppressor. Discov. Med. *10*, 322–328.

Wildin, R.S., Ramsdell, F., Peake, J., Faravelli, F., Casanova, J.L., Buist, N., Levy-Lahad, E., Mazzella, M., Goulet, O., Perroni, L., et al. (2001). X-linked neonatal diabetes mellitus, enteropathy and endocrinopathy syndrome is the human equivalent of mouse scurfy. Nat. Genet. *27*, 18–20.

Wysocka, J., Swigut, T., Xiao, H., Milne, T.A., Kwon, S.Y., Landry, J., Kauer, M., Tackett, A.J., Chait, B.T., Badenhorst, P., et al. (2006). A PHD finger of NURF couples histone H3 lysine 4 trimethylation with chromatin remodelling. Nature *442*, 86–90.

Yamane, K., Tateishi, K., Klose, R.J., Fang, J., Fabrizio, L.A., Erdjument-Bromage, H., Taylor-Papadimitriou, J., Tempst, P., and Zhang, Y. (2007). PLU-1 is an H3K4 demethylase involved in transcriptional repression and breast cancer cell proliferation. Mol. Cell *25*, 801–812.

Yu, J., Yu, J., Mani, R.S., Cao, Q., Brenner, C.J., Cao, X., Wang, X., Wu, L., Li, J., Hu, M., et al. (2010). An integrated network of androgen receptor, polycomb, and TMPRSS2-ERG gene fusions in prostate cancer progression. Cancer Cell *17*, 443–454.

Zheng, Y., Josefowicz, S.Z., Kas, A., Chu, T.T., Gavin, M.A., and Rudensky, A.Y. (2007). Genome-wide analysis of Foxp3 target genes in developing and mature regulatory T cells. Nature *445*, 936–940.

Zuo, T., Liu, R., Zhang, H., Chang, X., Liu, Y., Wang, L., Zheng, P., and Liu, Y. (2007a). FOXP3 is a novel transcriptional repressor for the breast cancer oncogene SKP2. J. Clin. Invest. *117*, 3765–3773.

Zuo, T., Wang, L., Morrison, C., Chang, X., Zhang, H., Li, W., Liu, Y., Wang, Y., Liu, X., Chan, M.W., et al. (2007b). FOXP3 is an X-linked breast cancer suppressor gene and an important repressor of the HER-2/ErbB2 oncogene. Cell *129*, 1275–1286.